BSGF - Earth Sciences Bulletin 2026, 197, 12

https://doi.org/10.1051/bsgf/2026003

Available online at:
www.bsgf.fr

Multidisciplinary approaches in metallogeny: for a global understanding of mineral systems : a tribute to Eric Gloaguen ; Eds : Giada Iacono, Florence Cagnard, Alain Chauvet, Yannick Branquet, Loïs Monnier, Johann Tuduri et Jérémie Melleton

OPEN ACCESS

Rare-metal mineralization and crust-derived magmatism in a collisional orogen: the Variscan metallogenic odyssey of the Sioule region (French Massif Central)

Christophe Ballouard[1,*], Patrick A. Carr[1], Loïs Monnier[2], Jean-Charles Fidalgo[1], Océane Rocher[1], Nicolas Esteves[3], Oscar Laurent[2], Marie Daoulas-Gérardin[1], Chantal Peiffert[1], Lou Declercq[1], Julien Mercadier[1], Alexis Plunder[4] and Jérémie Melleton[4]

[1] Université de Lorraine, CNRS, GeoRessources, F-54506, Vandoeuvre-lès-Nancy, France
[2] CNRS, Géosciences Environnement Toulouse (GET), Observatoire Midi-Pyrénées, 31400 Toulouse, France
[3] Université de Lorraine, CNRS, CRPG, F-54000 Nancy, France
[4] BRGM, F-45060 Orléans, France

Received: 3 November 2025 / Accepted: 26 February 2026 / Publishing online: 12 May 2026

Abstract – The Sioule region in the northern part of the French Massif Central of the Variscan belt hosts the Echassières complex, where a large W(-Sn) quartz vein system was intruded by the Beauvoir rare-metal granite (RMG) hosting disseminated Sn, Nb-Ta and Li mineralization. We combined whole-rock geochemical data, zircon U-Pb geochronology of migmatites and felsic igneous rocks of the Sioule area, along with U-Pb dating of cassiterite, wolframite, and apatite in the Echassières complex to reconstruct the regional magmatic and metallogenic evolution. Results reveal: (i) early W mineralization at 351 ± 9 Ma, coeval with peraluminous granite magmatism (Chantelle and St-Gervais massifs) and a N115-striking dextral shear zone; (ii) a second W mineralization phase at 329 ± 5 Ma, linked to rare-metal-rich rhyolitic dykes and the Colettes granite during NW-SE extension, synchronous with regional biotite microgranites (Pouzol-Servant Massif) and trachy-dacitic tuffs and lavas; and (iii) late-orogenic emplacement of the Beauvoir RMG with minor hydrothermal Sn and W at *ca.* 320-310 Ma, synchronous with biotite granites hosting quartz-tourmaline orbicules (Champs Massif) and pyroclastic flows. Our study reveals a 40 Myr-long metallogenic evolution with hydrothermal W mineralization preceding hydrothermal Sn and magmatic Li-Sn-Nb-Ta. Each mineralization period coincided with widespread crustal magmatism involving the anatexis of late-Ediacaran metasedimentary rocks and Cambrian-Ordovician metagranites, as shown by the dating of zircon in migmatites and inherited zircon in Variscan igneous rocks. However, rare-metal-enriched magmas remained spatially confined to the Echassières complex suggesting a structural corridor that repeatedly focused magmas and fluids from a localized fertile source.

Keywords: Peraluminous magmatism / Beauvoir rare-metal granite / W-Sn hydrothermal mineralization / plutonic-volcanic connection / migmatite / U-Pb geochronology

Résumé – Magmatisme crustal et minéralisations en métaux rares dans un orogène collisionnel : l'odyssée métallogénique de la région de la Sioule (Massif central français de la chaîne varisque). La région de la Sioule au nord du Massif central français de la chaîne varisque abrite le complexe d'Echassières, où un réseau de veines de quartz à W(-Sn), a été recoupé par le granite à métaux rares de Beauvoir, contenant une minéralisation disséminée à Li, Nb-Ta et Sn. Des analyses géochimiques (roche-totale) et géochronologiques (U-Pb sur zircon) des roches magmatiques felsiques et des migmatites de la zone de la Sioule ont été combinées à des datations U–Pb sur cassitérite, wolframite et apatite du complexe d'Echassières afin de reconstituer l'évolution magmatique et métallogénique régionale. Les résultats mettent en évidence : (i) un premier événement minéralisateur à W vers 351 ± 9 Ma, contemporain d'un cisaillement dextre N115 et de magmatisme granitique peralumineux (massifs de Chantelle et de

*Corresponding author: christophe.ballouard@univ-lorraine.fr

Saint-Gervais); (ii) une seconde phase de minéralisation à W à 329 ± 5 Ma, associée à l'intrusion de magmas riches en Li-Sn-W (massif granitique des Colettes et dykes rhyolitiques), synchrones d'un épisode plutonique-volcanique (microgranites à biotite de Pouzol–Servant et tufs trachy-dacitiques), dans un contexte extensif NO–SE; (iii) la mise en place du granite à métaux rares de Beauvoir, accompagnée d'une minéralisation hydrothermale à Sn (et W) vers 320 Ma, contemporaine de la cristallisation de granites à biotite, localement à orbicules de quartz-tourmaline (massif des Champs) et d'un volcanisme felsique explosif. Notre étude révèle une évolution métallogénique étalée sur 40 Ma. Chaque phase de minéralisation coïncide avec du magmatisme crustal impliquant l'anatexie de roches métasédimentaires tardi-édiacariennes et de métagranites cambro-ordoviciens, comme l'indiquent les âges U-Pb sur zircon de migmatites, et le zircon hérité des roches ignées varisques. Cependant, les magmas enrichis en métaux rares sont restés spatialement confinés au complexe d'Echassières, suggérant l'existence d'un couloir structural ayant concentré de manière répétée les magmas et les fluides issus d'une source fertile localisée.

Mots-clés : magmatisme peralumineux / granite à métaux rares de Beauvoir / minéralisation hydrothermale à W-Sn / connexion plutonique-volcanique / migmatite / géochronologie U-Pb

1 Introduction

Among orogenic mineralization, magmatic-hydrothermal Sn ± W deposits (*e.g.*, quartz veins, greisens, skarns) forming inboard of long-lived oceanic subduction zones or in continental collision zones are generally linked with reduced, evolved crustal granitic magmas (Romer and Kroner, 2016; Mao *et al.*, 2019; Lehmann, 2021; Gardiner *et al.*, 2024). Such Sn-W-fertile magmatism is associated to the partial melting of siliciclastic sediments, potentially pre-enriched in those elements through weathering processes (Romer and Kroner, 2015, 2016). Although W and Sn ores are commonly found spatially associated, deposits exhibiting significant concentrations of both metals are relatively rare (Sinclair *et al.*, 2014) reflecting the existence of processes able to fractionate Sn-from W. For instance, W and Sn can have contrasting behavior at the magmatic-hydrothermal transition due to generally higher aqueous fluid-melt partitioning for W compared to Sn (Schmidt *et al.*, 2020). Crustal melting processes may also fractionate W from Sn due to higher Sn incorporation in restitic biotite (Zhao *et al.*, 2022a). This could explain the temporal and spatial separation of Sn and W deposits in some metallogenic provinces suggesting a relationship between the thermal state of orogenic crust and the metallic signature of magmatic-hydrothermal deposits (Zhao *et al.*, 2022b; Harlaux *et al.*, 2023; Carr *et al.*, 2026).

Peraluminous rare-metal granites or pegmatites (RMGP) hosting magmatic disseminated Li, Nb, Ta, and Sn ore also represent typical deposits of hot orogens, and form from leucogranitic melts highly enriched in volatiles and fluxing elements such as F and Li (Černý and Ercit, 2005; Linnen and Cuney, 2005). Their emplacement dominantly occurs during late- to post-orogenic tectonics, in relation with extensional or transcurrent deformation (Cuney *et al.*, 2002; Melcher *et al.*, 2015; Huston *et al.*, 2023; Silva *et al.*, 2023; Gardiner *et al.*, 2024; Carr *et al.*, 2026; Černý *et al.*, 2026). The generation of rare-metal enriched melts is commonly ascribed to specific partial melting conditions and/or protoliths prevailing at the end of an orogen, typically, a high geothermal gradient superimposed on a mature crust that already experienced anatectic event(s). Suggested scenarios include (i) anatexis of unconventional metasedimentary rocks enriched in Li (*e.g.*, metabauxites; Horányi *et al.*, 2025), (ii) partial melting of crustal material pre-enriched in rare-metal, induced by metasomatism from mantle-derived hydrous mafic magmas (Smithies *et al.*, 2025), (iii) lower crustal granulite-facies metamorphism inducing the release of aqueous fluids enriched in biotite-hosted elements (LILE, HFSE and halogens) and enhancing partial melting of the overlying crust (Cuney and Barbey, 2014), (iv) re-melting of melt-depleted and rare-metal enriched lithologies at high-temperature (*i.e.*, restite melting) (Michaud *et al.*, 2021), (v) a combination of both previous scenarios involving the partial melting of biotite-rich residues induced by rare-metal-F-rich fluids (Simons *et al.*, 2016), and (vi) protracted crustal differentiation involving repeated stages of anatexis, and remelting of peraluminous (meta)granitic rocks (Ballouard *et al.*, 2023; Koopmans *et al.*, 2024; Carr *et al.*, 2026).

Although, most granites that have been genetically related to magmatic-hydrothermal Sn-W deposits lack disseminated rare-metal mineralization (Černý *et al.*, 2005), a spatial association is commonly observed between magmatic-hydrothermal W-Sn mineralization and RMGP either at the scale of a metallogenic field or a deposit. Such association is, for example, documented in the Archean North Pilbara Craton of Australia (Sweetapple and Collins, 2002), the Proterozoic Karagwe-Ankole Belt of Central Africa (Hulsbosch, 2019), and the Phanerozoic European Variscan belt including the Cornubian Batholith (Putzolu *et al.*, 2024), the Krušné Hory/Erzgebirge region (Breiter *et al.*, 1999; Burisch *et al.*, 2025), the Iberian Peninsula (Losantos *et al.*, 2025) and the French Massif Central (Marignac and Cuney, 1999). When magmatic-hydrothermal W-Sn mineralizations and RMGP occur together in a same deposit or district, they are commonly perceived contemporaneous and cogenetic resulting from a single main magmatic event (Hulsbosch *et al.*, 2016; Breiter *et al.*, 2017; Leopardi *et al.*, 2024). However, many deposits display complex crystallization sequences and/or fluid P-T evolutions, indicative of prolonged and multiphase histories (*e.g.*, Cathelineau *et al.*, 2020; Harlaux *et al.*, 2021; Meyer *et al.*, 2025). Geochronological advances, notably the increasing use of U-Pb dating on ore minerals (*e.g.*, wolframite and cassiterite), or skarn-related garnet, further reveal diachronous ore-forming processes, with hydrothermal W mineralization commonly preceding hydrothermal Sn and RMGP emplacement at both provincial and deposit scales (Burisch *et al.*, 2019; Reinhardt *et al.*, 2022; Harlaux *et al.*, 2023; Bermejo

et al., 2025; Carr *et al.*, 2026). This highlights the need to better resolve the temporal and genetic links between RMGP magmatism and W-Sn hydrothermalism, particularly in relation to regional tectonic-magmatic processes.

The Echassières complex (Sioule region) in the northern French Massif Central (FMC) exemplifies such a complex mineralization history and stands as an archetypal metallogenic district of the West European Variscan belt. In this area, the Beauvoir rare-metal granite (RMG), targeted for Li mining, hosts disseminated Li-micas (lepidolite), along with Sn (cassiterite) and Nb-Ta oxides (columbite-group minerals), and intrude, a wolframite-bearing quartz vein system mineralized with minor cassiterite (La Bosse stockwork; Aubert, 1969; Cuney *et al.*, 1992). Although, the late-Variscan emplacement of the Beauvoir RMG is well constrained at *ca.* 313 Ma based on multiple dating methods (Duthou and Pin, 1987; Cheilletz *et al.*, 1992; Melleton *et al.*, 2015; Rocher *et al.*, 2024; Esteves *et al.*, 2025a), the timing of W or Sn hydrothermalism remains controversial. U-Pb ages of the La Bosse stockwork and other W or Sn veins from the region, either obtained on wolframite or on texturally associated minerals such as monazite and rutile, range from *ca.* 330 to 310 Ma (Harlaux *et al.*, 2018; Carr *et al.*, 2021; Monnier *et al.*, 2021), with even earlier W mineralization event suspected before 360 Ma (Monnier *et al.*, 2021). Moreover, despite extensive research on the Beauvoir RMG—including the 1985 "*Géologie Profonde de la France*" deep drilling program (GPF, Cuney and Autran, 1987) and renewed interest driven by Li exploration—the timing and tectonic framework of granite magmatism across the Sioule region remain poorly constrained, with only sparse U-Pb dating available at the regional scale. This lack of chronological control limits our understanding of the geological processes governing W-Sn and RMGP mineralization at a crustal scale.

This study presents new age constraints on W-Sn and RMG mineralization in the Echassières complex based on U-Pb dating of apatite, wolframite and cassiterite. These results were combined with U-Pb zircon geochronology and whole-rock geochemistry on felsic igneous and metasedimentary rocks, including migmatites, from the Sioule region to clarify the links between tectono-magmatic events and the multiphase rare-metal metallogenic evolution.

2 Geological setting

2.1 The Northern French Massif Central in the West-European Variscan belt

The European Variscan belt is a hot orogen extending from the Bohemian massif in Central Europe to the Moroccan Meseta in North Africa that formed in relation with the late-Paleozoic collision between the two main continental masses Laurussia and Gondwana (Martínez Catalán *et al.*, 2021; Schulmann *et al.*, 2022; Cochelin *et al.*, 2025). The previously thickened, internal parts of the orogen host voluminous, dominantly peraluminous, early-Carboniferous to early-Permian granites and related RMGP and W-Sn deposits (Romer and Kroner, 2016). In the western part of the belt (Fig. 1a), including the FMC, and the Iberian and South Armorican massifs, RMGP belong to the peraluminous highly-phosphorous family of rare-metal granites (Linnen and Cuney, 2005) or the Li-Cs-Ta family of rare-metal pegmatites (Černý *et al.*, 2005). They were mostly emplaced between 320 and 300 Ma (Gourcerol *et al.*, 2019). The age of Sn and/or W-mineralized quartz veins, stockwork, or skarn deposits, are less well constrained but share a dominant late-Variscan context of emplacement (from 340 to 280 Ma; Carr *et al.*, 2021, 2026; Borrajo *et al.*, 2024; Bermejo *et al.*, 2025), generally associated to extensional or transcurrent tectonics (Schulmann *et al.*, 2022; Cochelin *et al.*, 2025).

In the FMC, most of the pre-Variscan crust consists of Ediacaran to late-Paleozoic metasedimentary rocks along with orthogneisses and (ultra)mafic rocks of Cambrian to Ordovician ages (Chelle-Michou *et al.*, 2017; Vanderhaeghe *et al.*, 2020; Laurent *et al.*, 2023). The orthogneiss protoliths correspond to former granitic plutons and felsic volcanic rocks of dominantly peraluminous compositions formed during two distinct tectonic-magmatic events (Melleton *et al.*, 2010; Ballèvre *et al.*, 2012; Chelle-Michou *et al.*, 2017; Couzinié *et al.*, 2017, 2022; Lotout *et al.*, 2017; Vanderhaeghe *et al.*, 2020; Couzinié and Laurent, 2021; García-Arias *et al.*, 2024). The first event (*ca.* 550-535 Ma) occurred in back-arc basins at the end of the Cadomian Orogeny, and the second (*ca.* 500-445 Ma) relates to the extension of the Gondwana margin coeval to the opening of the Rheic Ocean and possibly other narrow oceanic basins. In the North Armorican Massif, scarce magmatic-hydrothermal Sn-W mineralization is found associated with undeformed equivalents of late-Cadomian metagranites from the FMC (Chauris and Marcoux, 1994) (Fig. 1a).

Early oceanic subduction in the FMC is marked by high-pressure (HP) metamorphism of Ordovician (ultra)mafic igneous rocks at 390-360 Ma (Lotout *et al.*, 2020; de Hoÿm de Marien *et al.*, 2023). Related active margin magmatism is notably expressed in the northern FMC from 370 to 354 Ma, with the emplacement of calk-alkaline dioritic to tonalitic plutons (Bernard-Griffiths *et al.*, 1985; Berger *et al.*, 2024) and back-arc basin bimodal volcanism (Pin and Paquette, 1997). This mantle wedge-derived magmatism was sub-contemporaneous with crustal melting reflected by the emplacement at 360-350 Ma of cordierite-bearing peraluminous granitoids (CPG; Barbarin, 1999) such as the composite Guéret Massif (Cartannaz *et al.*, 2007b; Marcoux *et al.*, 2021).

The emplacement of the cordierite-bearing granitoids, synchronous with early N110-striking dextral shear zones (Cartannaz *et al.*, 2007b; Gébelin *et al.*, 2007, 2009), marks the end of nappe stacking tectonics that structured the FMC crust (Ledru *et al.*, 1989; Faure *et al.*, 2009). The upper part of the nappe stack, defining an inverted metamorphic sequence (see review in Vanderhaeghe *et al.*, 2020), corresponds to the Upper Gneiss Unit (UGU). It dominantly consists of migmatitic orthogneisses and paragneisses hosting relicts of HP eclogite- to granulite-facies metamorphic rocks. An Ordovician bimodal magmatic association with oceanic affinities, known as the "leptyno-amphibolitic complex" occurs at the base of the UGU. This complex overlies parautochtonous terrains composed of metasedimentary and felsic metaigneous rocks devoid of HP metamorphic records which include the Lower Gneiss Unit (LGU), and the lower grade Para-Autochthonous Unit (PAU).

The nappe stack is crosscut by the Sillon Houiller crustal discontinuity (Fig. 1a), a N20-striking sinistral fault, recording polyphase tectonic evolution with early ductile-brittle deformation before 330 Ma and late brittle reactivation at *ca.* 305 Ma (Thiery *et al.*, 2009). Ductile deformation along the Sillon Houiller is locally sealed by volcanic-sedimentary deposits

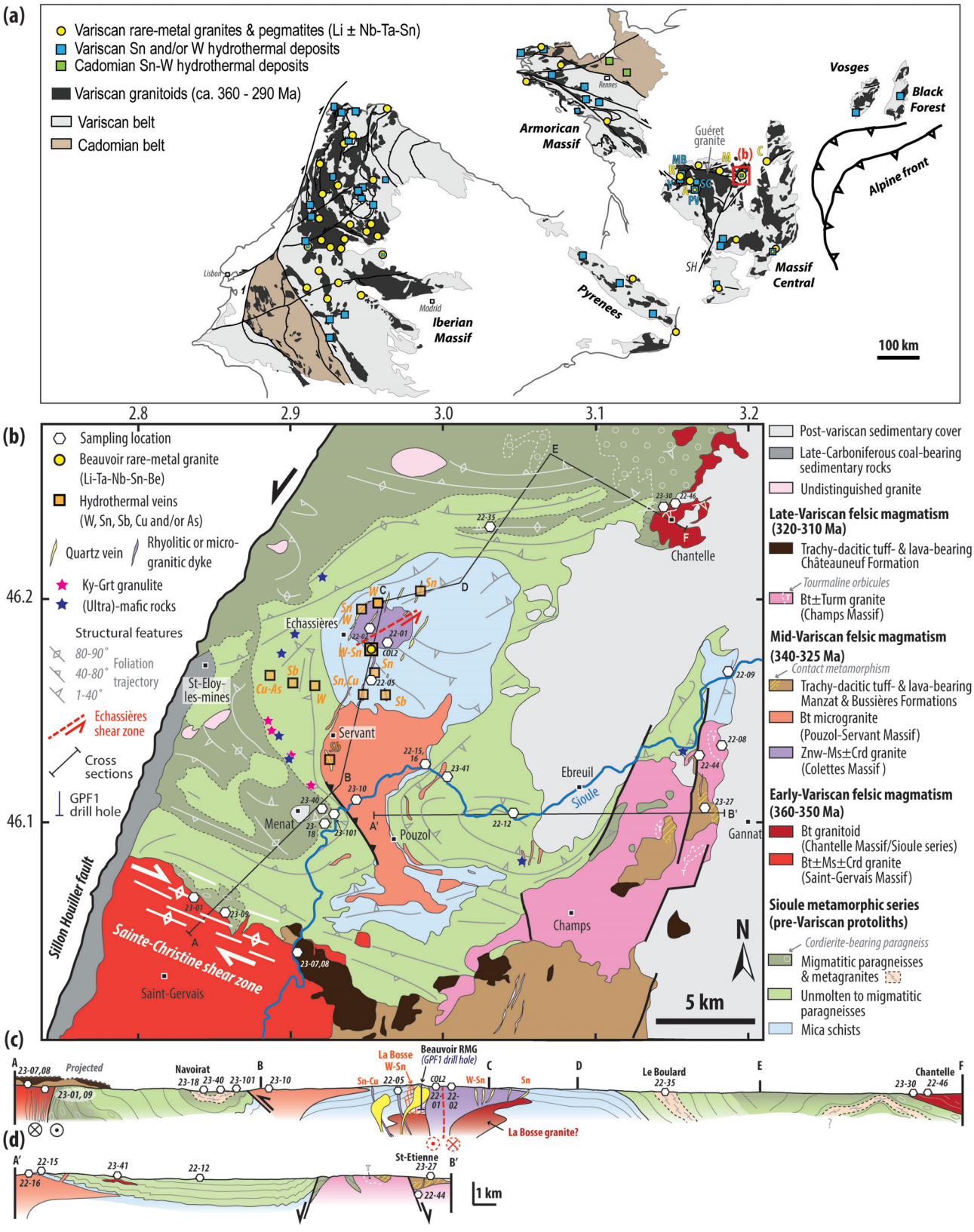

Fig. 1. Geological features of the Sioule region within the Variscan Belt. (a) Distribution of peraluminous rare-metal granites and pegmatites, and main hydrothermal Sn and/or W deposits in the western part of the European Variscan belt (based on Gourcerol *et al.*, 2021; Ballouard *et al.*, 2024; Borrajo *et al.*, 2024). Abbreviations: SH - Sillon Houiller fault, R - Richemont rare-metal rhyolite, A - Ambazac rare-metal pegmatite field, M - Montebras rare-metal granite, C - Chavence rare-metal granite. (b) Geological map and (c-d) cross sections of the Sioule region (based on Grolier, 1971; Cuney and Autran, 1987; Feybesse and Teygey, 1987; Thiéry, 2012, regional geological maps at the 1:50,000 scale, and own field observations). The Echassières shear zone is from Gagny and Jacquot (1987). Mineral abbreviations follow Warr (2021). Other abbreviation: RMG - Rare-metal granite.

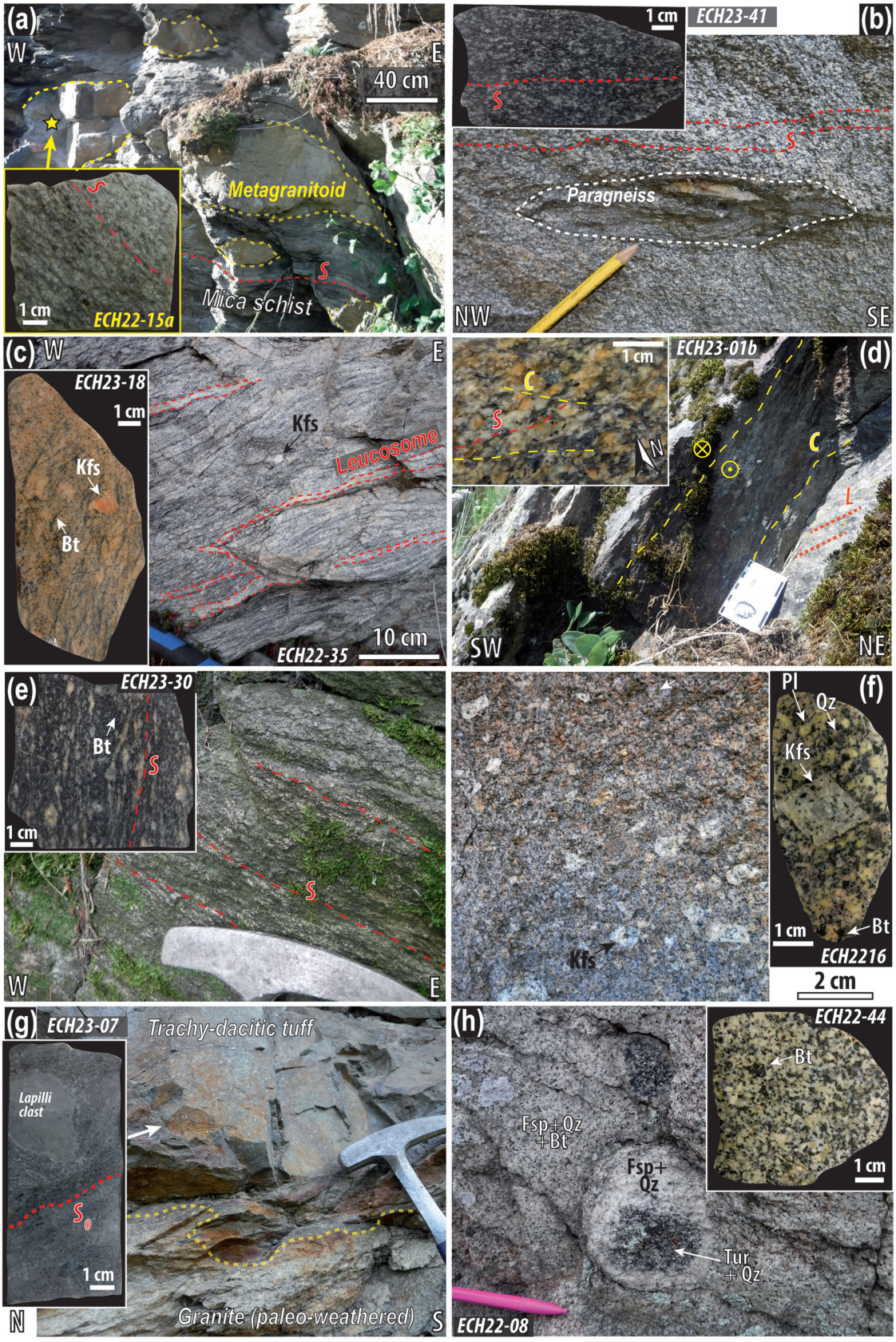
(a)
W
E
40 cm
Metagranitoid
S
Mica schist
1 cm
ECH22-15a
(b)
1 cm
ECH23-41
S
Paragneiss
NW
SE
(c)
W
E
ECH23-18
1 cm
Kfs
Bt
Kfs
Leucosome
ECH22-35
10 cm
(d)
1 cm
ECH23-01b
C
S
N
C
L
SW
NE
(e)
ECH23-30
Bt
S
1 cm
S
W
E
Kfs
(f)
Pl
Qz
Kfs
1 cm
Bt
ECH2216
2 cm
(g)
ECH23-07
Trachy-dacitic tuff
Lapilli clast
S_0
1 cm
N
Granite (paleo-weathered)
S
(h)
ECH22-44
Bt
1 cm
Fsp+Qz +Bt
Fsp+ Qz
Tur + Qz
ECH22-08

Fig. 2. Field and hand sample photographs of felsic (meta-)igneous rocks from the Sioule region. (a) Boudins of muscovite ± biotite metagranitoid hosted by mica schist (Sioule Valley; WGS84 coordinates: 2.9897; 46.1250). (b) Paragneiss enclave within a meter-sized body of moderately deformed biotite granitoid (Sioule Valley; 3.0029; 46.1194). (c) Metatexitic biotite metagranite with scarce K-feldspar phenocrysts, layered with granitic leucosomes bordered by biotite ribbons (Le Boulard quarry; 3.0313, 46.2324). The inset shows a diatexitic metaleucogranite with partially resorbed K-feldspar phenocrysts. (d) Saint-Gervais biotite-cordierite-muscovite granite displaying C/S fabrics with dextral kinematics along the Sainte-Christine shear zone (Sainte-Christine; 2.8373; 46.0642). (e) Biotite granitoid of the Chantelle Massif with roughly defined foliation (3.1522, 46.2435). (f) Pouzol-Servant K-feldspar porhyritic biotite microgranite (Sioule Valley; 2.9876, 46.1253). (g) Unconformable contact between trachy-dacitic tuff of the Châteauneuf Formation and paleo-weathered Saint-Gervais granite (Pont de Braynant; 2.9053, 46.0364). Note lapilli clast mostly consisting of devitrified glass in bedded tuff ECH23-07. (h) Champs biotite granite (ECH22-44) including leucogranitic facies with quartz-tourmaline orbicules (ECH22-08; 3.1813, 46.1317). Mineral abbreviation from Warr (2021). Other abbreviations: S_0 - bedding, S - foliation, C - shear plane, L - lineation.

(the regionally known "Tufs anthracifères" series), dated between 337 ± 3 and 326 ± 3 Ma (Bruguier *et al.*, 1998; Cartannaz *et al.*, 2007a; Thiery *et al.*, 2009). The deposition of volcanic material has been attributed in the northeastern FMC to the formation of a N70- to N50-trending graben (Bertaux *et al.*, 1993). Moreover, on the western side of the Sillon Houiller Fault, the interbedding of these volcanic rocks with limestone indicates deposition in lagoonal environments sporadically invaded by the sea (Hottin *et al.*, 1991; Quenardel *et al.*, 1991), collectively pointing to major crustal extension at that time.

From *ca.* 335 to 300 Ma, granitic magmatism in the eastern FMC progressively propagated from north to south, possibly in relation to southward delamination of the lithospheric mantle (Laurent *et al.*, 2017). During this period, the emplacement of muscovite- and cordierite-bearing peraluminous granites (MPG and CPG; Barbarin, 1999), dominantly sourced from metasedimentary rocks and orthogneisses, was contemporaneous with the intrusion of Mg-K-rich mafic igneous rocks (vaugnerites) reflecting the partial melting of metasomatized mantle, and K-feldspar porphyritic calc-alkaline granites of likely hybrid origin (Couzinié *et al.*, 2016; Laurent *et al.*, 2017; Moyen *et al.*, 2017; Werle *et al.*, 2023). Granite emplacement in the northern FMC around 325-310 Ma was notably accommodated by N-S striking detachment and NW-SE-orientated dextral strike-slip fault systems (Gébelin *et al.*, 2009), while in the southern FMC, extensional tectonics have controlled the exhumation of domes cored by migmatites until *ca.* 295 Ma (Vanderhaeghe *et al.*, 2020).

In the FMC, most of the *ca.* 315-310 Ma RMGP are located in the northern part of the massif and define a *ca.* 150 km long, approximately W-E-trending belt including the Richemont rare-metal rhyolite dyke, the Chédeville LCT pegmatites of the Ambazac pegmatite field as well as the Montebras, Beauvoir and Chavence rare-metal granites (Fig. 1a) (Marignac and Cuney, 1999; Gourcerol *et al.*, 2019; Harlaux *et al.*, 2025). The ore assemblage of RMPG primarily consists of lepidolite, Li-Al-phosphates (amblygonite-group minerals), cassiterite and columbite-group minerals. Although W and/or Sn magmatic-hydrothermal deposits show a more widespread geographic distribution, wolframite ± cassiterite ± scheelite mineralizations mostly dated between 320 and 310 Ma are particularly abundant in the northern FMC (Marignac and Cuney, 1999; Cuney *et al.*, 2002; Harlaux *et al.*, 2015, 2018, 2021; Carr *et al.*, 2021). Notable occurrences include the Moullin-Barret and Vaulry quartz vein networks near the Richemont dyke, the quartz veins of St-Goussaut east of the Chédeville pegmatites, the Puy-les-Vignes breccia pipe (and suspected concealed RMG) and the stockwork and quartz veins of the Sioule region (Fig. 1a-b).

2.2 Tectonic-metamorphic and magmatic evolution of the Sioule region

The Sioule region is bounded to the west by the Sillon Houiller fault and to the east by normal faults of the Ebreuil and Limagne grabens accommodating the deposition of Oligocene sediments (Fig. 1b-d). In the Sioule area, two-mica ± staurolite schists with mostly gently dipping foliation (Fig. 2a) crop out in antiformal structures and are overlain by higher-grade gneisses bearing biotite, muscovite, sillimanite, kyanite, garnet and/or cordierite (Fig. 2b-c) (Grolier, 1971; Thiéry, 2012). The inverted metamorphic gradient has been interpreted as evidence for thrusting (Feybesse and Teygey, 1987; Ledru *et al.*, 1989), with a nappe stack consisting from bottom to top of PAU mica schists, LGU unmolten to slightly migmatitic paragneisses, and UGU migmatitic paragneisses (Schulz *et al.*, 2001; Schulz, 2009). In this model, lenses of (ultra)mafic rocks, marbles and garnet-kyanite granulitic rocks within the gneisses (Fig. 1b) (Grolier, 1971; Ravier and Chenevoy, 1979) mark the base of the UGU (Do Couto *et al.*, 2016). The Sioule metamorphic rocks record a complex multistage tectonic-metamorphic evolution. The dominant WNW-ESE-striking stretching lineation developed in the foliation of most units and associated with top-to-the-WNW kinematic was attributed to nappe formation and exhumation (Audren *et al.*, 1987; Feybesse and Teygey, 1987; Schulz, 2009; Do Couto *et al.*, 2016). The minimum age of related MP-MT Barrovian metamorphism and partial melting (peak P-T of ~10 kbar and 800 °C, Schulz, 2001) is poorly constrained by monazite chemical dating between 415 and 330 Ma and U-Pb dating of zircon from garnet-kyanite granulite from 340 to 330 Ma (Schulz, 2009; Do Couto *et al.*, 2016). Moreover, a later deformation event at lower pressure notably expressed in the southern part of the region and associated with top-to-the-SE kinematic, was either attributed to contractional (Feybesse and Teygey, 1987; Schulz, 2009) or extensional tectonics (Faure *et al.*, 1993). Biotite Ar-Ar ages of Sioule metamorphic rocks ranging from 335 to 330 Ma were interpreted as related to rock exhumation and cooling occurring during this later deformation event (Faure *et al.*, 2002).

To the south, the N110-N120-striking dextral Sainte-Christine shear zone affects the Sioule metamorphic rocks, including migmatites, and biotite ± cordierite ± muscovite ± amphibole-bearing, granitoids of the Saint Gervais Massif (Barbarin and Belin, 1982; Hottin *et al.*, 1989) (Fig. 2d). The minimum age of strike-slip deformation is constrained by ^{40}Ar-^{39}Ar dating of biotite from mylonitic granitoid at *ca.* 338-335 Ma (Faure *et al.*, 2002) as well as the unconformable deposition of volcanic-sedimentary rocks that were assigned to the regional *ca.* 335 Ma old "Tufs anthracifères series"

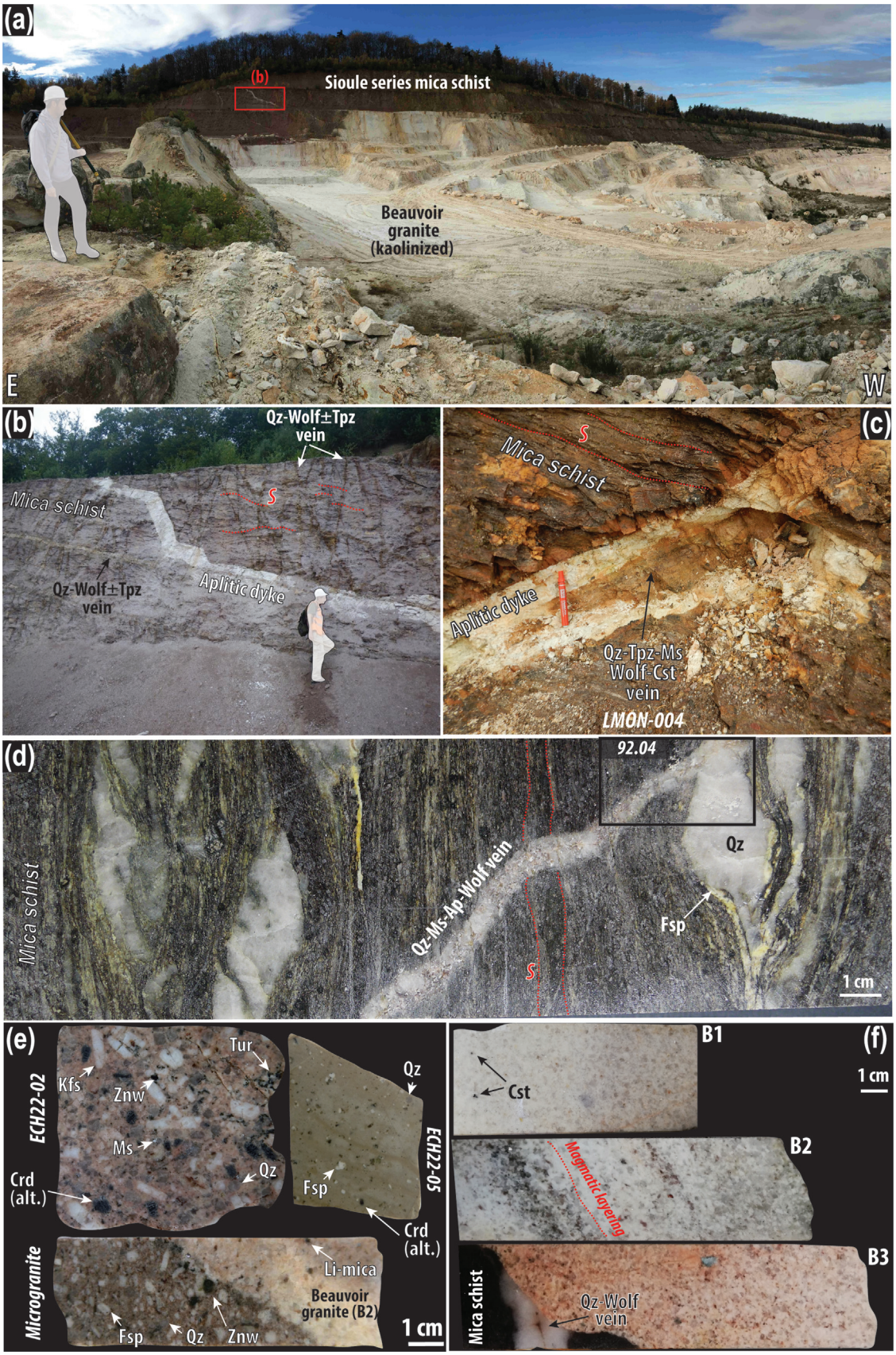
(a)
(b)
Sioule series mica schist
Beauvoir granite (kaolinized)
E
W
(b)
Qz-Wolf±Tpz vein
Mica schist
S
Qz-Wolf±Tpz vein
Aplitic dyke
(c)
S
Mica schist
Aplitic dyke
Qz-Tpz-Ms Wolf-Cst vein
LMON-004
(d)
92.04
Qz
Mica schist
Qz-Ms-Ap-Wolf vein
Fsp
S
1 cm
(e)
ECH22-02
Tur
Kfs
Znw
Ms
Qz
Crd (alt.)
Qz
Fsp
ECH22-05
Crd (alt.)
Li-mica
Beauvoir granite (B2)
Micrognanite
Fsp
Qz
Znw
1 cm
(f)
B1
Cst
1 cm
B2
Magmatic layering
B3
Mica schist
Qz-Wolf vein

Fig. 3. Field and hand sample photographs of the Echassières complex. (a) Kaolinized apical zone of the Beauvoir rare-metal granite and its mica schist host (Beauvoir open pit; WGS84 coordinates: 2.9563, 46.1767). (b) La Bosse stockwork with quartz-wolframite veins and aplitic dyke crosscutting the mica schists above the Beauvoir granite (2.9549, 46.1756). (c) Raft of quartz-wolframite-cassiterite vein (LMON-004) within an aplitic dyke of the La Bosse stockwork. (d) GPF drill core of Sioule series mica schist with quartz ± feldspar lenses parallel to the foliation, crosscut by a slightly folded quartz-muscovite-apatite-wolframite vein (92.04 m). (e) Colettes K-feldspar porphyritic muscovite-zinnwaldite-cordierite granite (ECH22-02) as well as microgranitic and rhyolitic sub-equivalents. The zinnwaldite-muscovite porphyritic microgranite occurs as enclave in the B2 unit of the Beauvoir granite (GPF drill core - 700m). The devitrified porphyritic rhyolite (ECH22-05) occurs as partially silicified dyke to the south of the Echassières complex. It hosts clusters of muscovite likely representing pseudomorphs after cordierite (See Fig. S3h). (f) GPF drill core of the B1 (132.85 m), B2 (642.8 m) and B3 (874.3 m) units of the Beauvoir RMG, illustrating disseminated cassiterite, magmatic layering and the crosscutting relationship between the B3 Beauvoir granite unit and quartz-wolframite vein in the mica schist. Mineral abbreviation from Warr (2021). Other abbreviation: S - foliation, Wolf - wolframite.

(Grolier, 1971). The biotite granitoids of the Chantelle Massif located northeast of the region also show evidence of solid-state deformation, and exhibit variably developed, shallowly dipping foliation and mineral lineation (Fig. 2e) (Grolier, 1971).

The Sioule mica schists in the central part of the region were intruded by the strongly K-feldspar porphyritic, biotite microgranite of the Pouzol-Servant Massif (Fig. 2f), as well as by the granites of the Echassières granitic complex, which include the Li-rich K-feldspar porphyritic two-mica and cordierite Colettes granite and the Beauvoir RMG (Aubert, 1969) (Fig. 3). The Rb-Sr whole-rock isochron ages obtained on the Pouzol-Servant microgranite and Colettes granite are of 335 ± 9 and 317 ± 8 Ma, respectively (Pin, 1991; recalulated using ^{87}Rb decay constant of Villa *et al.*, 2015). As reported by Grolier (1971), the Pouzol-Servant laccolith is thrust over the Sioule mica schists on its western side, and Gagny and Jacquot (1987) suggested that the rotation of sub-vertical magmatic fabrics in the Colettes granite reflects its emplacement during sinistral movement along a N60-striking shear zone. In contrast, Faure *et al.* (1993) argued that the asymmetrical shape of the Pouzol-Servant and Colettes granites is consistent with an emplacement during a regional NW-SE extension event, similar to that documented in the Montmarault granite, located west of the Sillon Houiller fault (Joly *et al.*, 2007, 2008). Such extension would be coeval with felsic volcanism of the "Tufs anthracifères series" represented by the biotite ± amphibole ± clinopyroxene trachy-dacitic tuffs and lavas of the Manzat, Bussière, and Châteauneuf Formations (Figs. 1 and 2g) (Alsac *et al.*, 1988).

To the east, the biotite granites of the Champs Massif dated using the biotite ^{40}Ar-^{39}Ar method at 322.3 ± 1.2 Ma, developed a metamorphic aureole in trachy-dacitic tuffs and lavas (Fig. 1b, d) (Faure *et al.*, 2002). They have an equigranular to porphyritic texture and include a leucocratic facies bearing quartz-tourmaline orbicules (Grolier, 1971) (Fig. 2h).

2.3 The Echassières complex

The Echassières granitic complex has been estimated from gravimetric data to be up to 5 km thick, with a lateral extent of ~6 km, significantly exceeding the current surface outcrop (Vigneresse, 1987) (Fig. 1b-c). The complex lies at the center of a major field of quartz veins, accompanied by subordinate microgranite, rhyolite (Fig. 3e) and lamprophyre dykes. The veins and dykes dip at low to high angle and are prominently oriented between N10 and N40 (Aubert, 1969) (Fig. 1b-c). Several veins are mineralized with wolframite and, less frequently, contain cassiterite, topaz, arsenopyrite, and stibnite, as well as Cu- and Pb-bearing ore minerals (Aubert, 1969). The main and most complex mineralized system, the La Bosse stockwork, located at the southern border of the Colette granite, consists of wolframite-bearing quartz veins that are predominantly oriented sub-parallel to the gently dipping mica schist foliation, and interconnected by steeper oblique veins (Fig. 3a-d and Supplementary Fig. S2) (Aubert, 1969; Jacquot and Gagny, 1985; Aïssa *et al.*, 1987a). This network both intersects and is crosscut by pegmatite and aplite dykes (Fig. 3a-c), some of which are mineralized with cassiterite and topaz. Late hydrothermal overprints include topaz ± Li-F-mica veins, pervasive topazification, and emplacement of greisen-like veins containing a mica + quartz ± apatite ± topaz assemblage (Fig. 3d) (Aubert, 1969; Aïssa *et al.*, 1987a; Monnier *et al.*, 2019). Three generations of wolframite, characterized by distinct Fe/Mn ratios have been identified within the stockwork and other vein systems in the region, reflecting at least three separate hydrothermal episodes (Monnier *et al.*, 2019).

U-Pb dating of monazite from the alteration halo of a wolframite-mineralized topaz vein in the stockwork yielded ages of 355 ± 6 and 336 ± 3 Ma, whereas W-rich rutile and monazite from the halo of the Sn-W-mineralized Suchot vein, located at the contact between the Colettes granite and mica schists, returned ages from 331 ± 5 to 307 ± 3 Ma (Monnier *et al.*, 2021). The earliest wolframite crystallization was suggested by the authors to have occurred prior to 355 Ma (interpreted as the age of mica schist metamorphism) while the ca. 330 Ma age, attributed to topazification, was considered as the main wolframite mineralizing event. In contrast, a *ca.* 310 Ma age was linked to hydrothermal activity associated with the emplacement of the Beauvoir RMG (Monnier *et al.*, 2021). U-Pb dating of stockwork wolframite by ID-TIMS yielded an age of 334.4 ± 1.7 Ma (Harlaux *et al.*, 2018). This age was later contested by Carr *et al.* (2021), who suggested an inappropriate common Pb correction and instead proposed an age of 316.7 ± 5.8 Ma, based on LA-ICP-MS U-Pb data.

The La Bosse stockwork was thought to be related to an inferred blind intrusion (labelled "La Bosse granite"; Fig. 1c) although such a unit was never intersected by the 900 m deep GPF1 scientific drill hole (Cuney and Autran, 1987). The stockwork, for which the depth of formation is estimated between 3.7 and 4.5 km (1.0-1.2 kbar) based on fluid inclusions analyses (Aïssa *et al.*, 1987b), is crosscut by both the Colettes and Beauvoir granites (Aubert, 1969) (Figs. 1c and

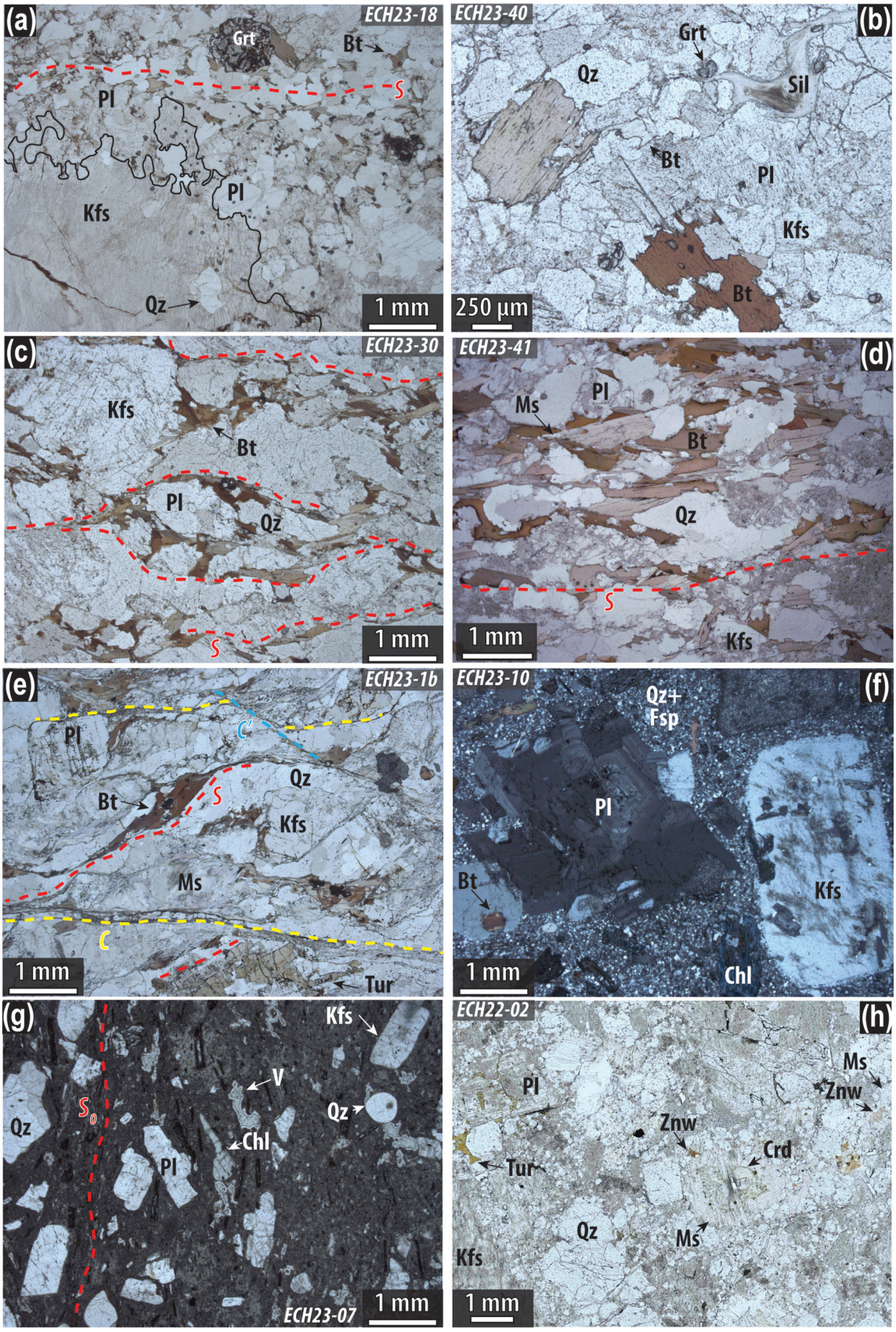
(a)
ECH23-18
Grt
Bt
Pl
S
Pl
Kfs
Qz
1 mm
(b)
ECH23-40
Grt
Qz
Sil
Bt
Pl
Kfs
Bt
250 µm
(c)
ECH23-30
Kfs
Bt
Pl
Qz
S
1 mm
(d)
ECH23-41
Pl
Ms
Bt
Qz
S
1 mm
Kfs
(e)
ECH23-1b
Pl
C'
Qz
Bt
S
Kfs
Ms
C
1 mm
Tur
(f)
ECH23-10
Qz+
Fsp
Pl
Bt
Kfs
1 mm
Chl
(g)
Kfs
V
Qz
S_0
Qz
Chl
Pl
ECH23-07
1 mm
(h)
ECH22-02
Ms
Pl
Znw
Znw
Crd
Tur
Qz
Ms
Kfs
1 mm

Fig. 4. Petrographic and textural features of studied felsic (meta-)igneous rocks. (a-b) Migmatitic biotite-garnet ± sillimanite metaleucogranites, with a perthitic K-feldspar phenocryst corroded by lobate quartz and plagioclase in (a). (c-d) Moderately deformed biotite granitoid from the Chantelle Massif (ECH23-30) and from a meter-sized igneous body in the Sioule Valley (ECH23-41). (e) Biotite-muscovite-tourmaline granite of the St-Gervais Massif displaying C/S fabrics and containing muscovite agglomerates interpreted as pseudomorphs after cordierite. (f) Porphyritic biotite microgranite of the Pouzol-Servant Massif, displaying phenocrysts and glomerocrysts of feldspar, quartz and biotite ± chlorite within a microgranular groundmass consisting of quartz and feldspar (cross-polarized light). (g) Trachy-dacitic ash flow tuff of the Châteauneuf Formation consisting of locally broken phenocrysts of quartz, feldspar and chlorite, vesicles (V) partially filled with mosaic quartz (possible devitrified glass shards) and an altered ground mass hosting aligned microlitic feldspar. Flow bedding (S_0) is notably marked by altered, unidentified, black minerals. (h) Two-mica-cordierite granite of the Colettes Massif. Cordierite is partially replaced by gigantolite, an assemblage of zinnwaldite and muscovite, and zinnwaldite commonly cores muscovite flakes. Secondary tourmaline occurs as crack filling. Mineral abbreviation from Warr (2021).

3a). Mica schist enclaves hosting wolframite ± cassiterite-bearing quartz veins are found as rafts in the Beauvoir intrusion down to the bottom of the GPF1 drill hole (Figs. 3f and S2). The emplacement depth of the Beauvoir RMG was estimated to be ~3km (0.8 kbar; Aïssa *et al.*, 1987b). The Beauvoir RMG is a typical example of an incrementally-constructed pluton, as the three main magmatic units (Figs. 3f and S2) that were originally recognized (from bottom to top: B3, B2 and B1; Cuney *et al.*, 1992; Raimbault *et al.*, 1995) have been subdivided into eighteen compositionally different sills (Esteves *et al.*, 2025b). The whole granite hosts lepidolite along with amblygonite-group minerals, topaz, cassiterite, and columbite-group minerals. However, the proportion of rare-metal- and F-rich minerals increase toward the apical part of the granite (B1 unit), representing the most evolved, incompatible element-enriched and Fe-depleted, magma batch. Moreover, lenses of microgranite with porphyritic texture, also referred as Beauvoir porphyry enclaves (Monnier *et al.*, 2018), occur in the B2 and B3 units (Raimbault *et al.*, 1995) (Figs. 3e and S2). The whole-rock composition and the quartz trace element signature of the microgranite enclaves is similar to the Colettes granite (Raimbault and Azencott, 1987; Monnier *et al.*, 2018). While the Beauvoir RMG induced sodic metasomatism of the Colettes granite (Aubert, 1969; Raimbault *et al.*, 1995), the Beauvoir intrusion and its host rocks are notably crosscut by a series of mostly sub-vertical and NE-SW-striking quartz veins, associated to greisen alteration and causing the replacement of magmatic lepidolite and feldspar by a quartz-muscovite ± apatite ± cassiterite assemblage (Aubert, 1969; Merceron *et al.*, 1992; Monnier *et al.*, 2021) (Fig. S2). This magmatic-hydrothermal event, dated in the Echassières complex between 314.3 ± 5.5 and 307 ± 3 Ma using U-Pb on apatite and monazite, respectively, was sub-synchronous with the emplacement of the Beauvoir RMG (Monnier *et al.*, 2021; Rocher *et al.*, 2024). The latter is notably constrained at 313.4 ± 1.3 Ma based on ID-TIMS U-Pb analyses of magmatic apatite (Esteves *et al.*, 2025a). Several late hydrothermal episodes affected the Beauvoir RMG during the Permian and Mesozoic (Rocher *et al.*, 2024), before intense weathering, presumably during the Tertiary, led to pervasive kaolinization of its apical zone (Fig. 3a).

3 Samples and analytical methods

Several samples of felsic igneous rocks were analyzed for whole-rock geochemistry (n =19) and zircon U-Pb geochronology (n=12) (Figs. 1b-d and 2). The new geochemical data are compared with those compiled from the literature (mostly major element compositions) reported in Supplementary file (Tab. S9). In addition, we examined the U-Pb detrital zircon record of three metasedimentary samples: one quartzite from the mica schist unit (ECH22-09) and two samples from the overlying paragneiss unit, including a quartzite (ECH22-12b) and a paragneiss (ECH23-101) (See Fig. S3a-b). Several W- and/or Sn-mineralized samples from the Echassières complex were also collected from the GPF1 drill core for *in situ* U-Pb dating of wolframite, cassiterite, and apatite (see sample location in cross section of Fig. S2). They include a quartz-muscovite-apatite-wolframite vein (GPF-92.04, Fig. 3d) crosscutting the mica schists above the Beauvoir intrusion, a quartz-mica-cassiterite veinlet with minor wolframite (P45b) hosted in a mica schist enclave within the Beauvoir RMG, and the cassiterite-mineralized B1, B2 and B3 facies of the Beauvoir RMG (Fig. 3f). Additionally, a wolframite-cassiterite-bearing quartz-topaz-muscovite vein, crosscutting mica schists and occurring as a raft in an aplitic dyke of the La Bosse stockwork, was sampled near the top of the Beauvoir granite open pit (LMON-004, Fig. 3c). Finally, both zircon and apatite U-Pb dating were performed on the Colettes granite (ECH22-02 for zircon, Fig. 3e; and COL2 for apatite, see Fig. 5A in Monnier *et al.*, 2018), along with apatite U-Pb analyses of its microgranitic sub-equivalent, found as an enclave within the B3 facies of the Beauvoir RMG (P51; see Fig. 5D in Monnier *et al.*, 2018).

The GPS coordinates of the samples, along with detailed analytical protocols, whole-rock geochemical data for the felsic igneous rocks, and U-Pb isotopic data (including results obtained on reference materials) are provided in the Supplementary files. Only a short summary of analytical protocols is provided in the following. Prior to dating, the internal textures of most minerals were imaged using cathodoluminescence (CL), except wolframite, imaged using backscattered electron (BSE) imaging and energy-dispersive spectrometry (EDS) chemical mapping. U-Pb isotopic compositions were determined by LA-ICP-MS using matrix-matched reference materials. Raw data were processed in Iolite4 (Paton *et al.*, 2010) with the U-Pb Geochronology data reduction scheme (DRS) for zircon and apatite, and VizualAge_UcomPbine DRS (Petrus and Kamber, 2012) for wolframite and cassiterite. A matrix correction factor was determined offline for apatite using three reference materials (Rocher *et al.*, 2024). U-Pb diagrams and ages were produced using *IsoplotR* (Vermeesch, 2018) with uncertainties quoted at the 2σ level. The long-term reproducibility of secondary reference materials, combined in quadrature is included.

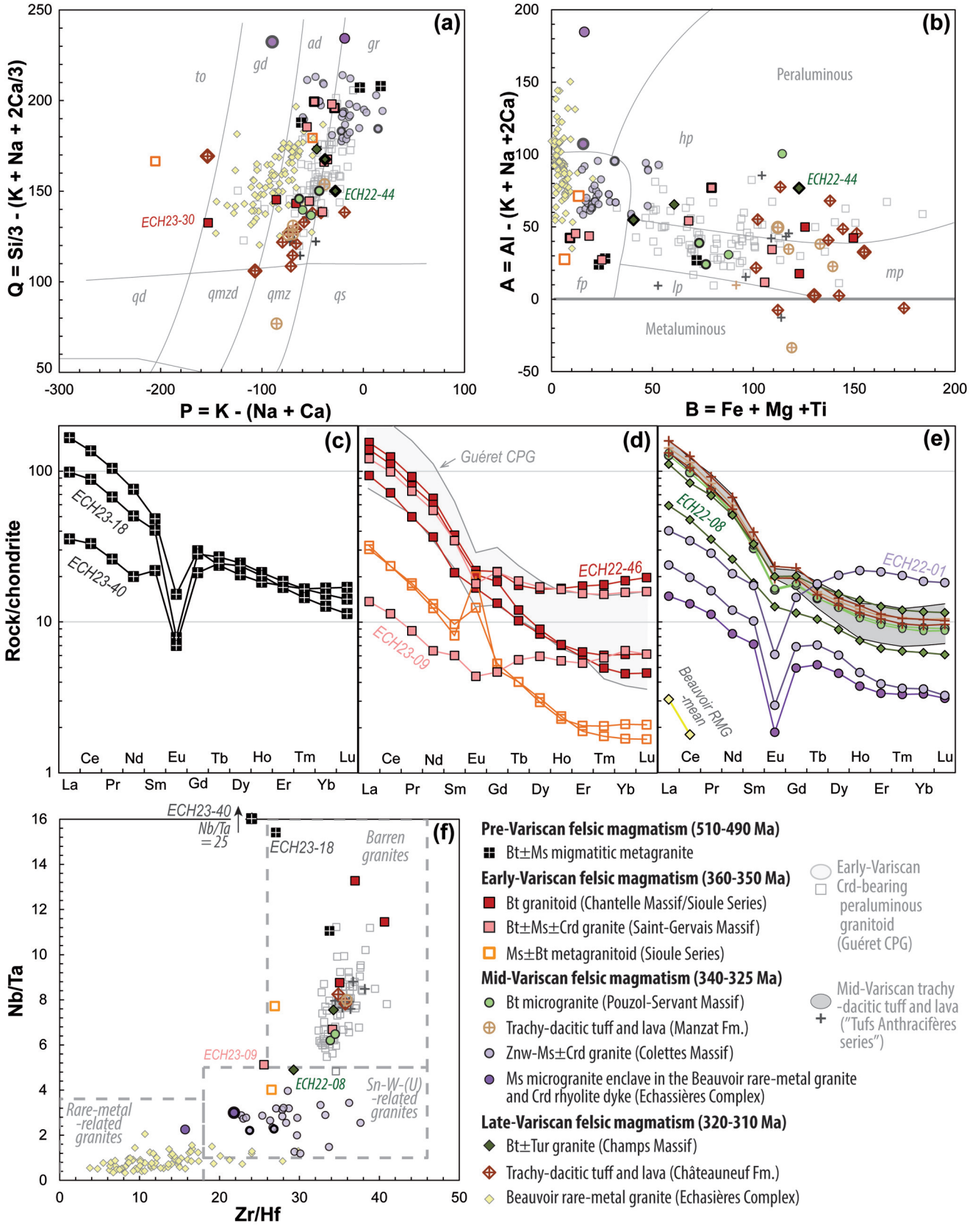
(a)
Q = Si/3 - (K + Na + 2Ca/3)
P = K - (Na + Ca)
to
gd
ad
gr
qd
qmzd
qmz
qs
ECH23-30
ECH22-44
(b)
A = Al - (K + Na +2Ca)
B = Fe + Mg +Ti
Peraluminous
Metaluminous
hp
mp
lp
fp
ECH22-44
(c)
Rock/chondrite
ECH23-18
ECH23-40
(d)
Guéret CPG
ECH22-46
ECH23-09
(e)
ECH22-08
ECH22-01
Beauvoir RMG -mean
La Pr Sm Gd Dy Er Yb
Ce Nd Eu Tb Ho Tm Lu
(f)
Nb/Ta
Zr/Hf
ECH23-40
Nb/Ta =25
ECH23-18
Barren granites
ECH23-09
ECH22-08
Sn-W-(U) -related granites
Rare-metal -related granites
Pre-Variscan felsic magmatism (510-490 Ma)
Bt±Ms migmatitic metagranite
Early-Variscan felsic magmatism (360-350 Ma)
Bt granitoid (Chantelle Massif/Sioule Series)
Bt±Ms±Crd granite (Saint-Gervais Massif)
Ms±Bt metagranitoid (Sioule Series)
Mid-Variscan felsic magmatism (340-325 Ma)
Bt microgranite (Pouzol-Servant Massif)
Trachy-dacitic tuff and lava (Manzat Fm.)
Znw-Ms±Crd granite (Colettes Massif)
Ms microgranite enclave in the Beauvoir rare-metal granite and Crd rhyolite dyke (Echassières Complex)
Late-Variscan felsic magmatism (320-310 Ma)
Bt±Tur granite (Champs Massif)
Trachy-dacitic tuff and lava (Châteauneuf Fm.)
Beauvoir rare-metal granite (Echasières Complex)
Early-Variscan Crd-bearing peraluminous granitoid (Guéret CPG)
Mid-Variscan trachy -dacitic tuff and lava ("Tufs Anthracifères series")

Fig. 5. Whole-rock geochemical features of felsic (meta-)igneous rocks from the Sioule region, with (a-b) major element compositions shown in Q-P (Debon and Le Fort, 1988) and A-B (Villaseca *et al.*, 1998) chemical-mineralogical diagrams, (c-e) REE compositions in chondrite-normalized (Palme and O'Neill, 2014) diagrams, and (f) HFSE fractionation degree in the Nb/Ta *versus* Zr/Hf diagram (Ballouard *et al.*, 2016). For comparison, the composition of early-Variscan cordierite-bearing peraluminous granitoids (CPG) of the Guéret Massif and mid-Variscan trachy-dacitic tuffs and lavas ("Tufs anthracifères" series) occurring west of the Sillon Houiller fault are also shown (Cartannaz, 2006). Abbreviations: (a) to - tonalite, gd - granodiorite, ad - adamellite (monzogranite), gr - granite, qd - quartz diorite, qmzd - quartz monzodiorite, qmz – quartz monzonite, qs - quartz syenite; (b) fp - felsic peraluminous, lp - low peraluminous, mp - moderately peraluminous, hp - highly peraluminous. Samples from this study are shown in bold only when compared to those from the literature.

Individual dates are presented for concordant data (≥ 90%) and are derived from $^{207}Pb/^{206}Pb$ dates when older than 1000 Ma, and $^{206}Pb/^{238}U$ dates when younger.

4 Results

4.1 Petrographic and geochemical characteristics of felsic igneous rocks from the Sioule region

Voluminous bodies of migmatitic orthogneiss (at least several meters thick), previously mapped as migmatitic paragneisses in the literature, were identified within the paragneiss units, notably in the southwestern (samples ECH23-18 and ECH23-40) and northern parts of the study area (sample ECH22-35; Figs. 2c and S3c-d). The biotite orthogneisses, which also contain minor, mostly secondary muscovite, host sparse and partially resorbed perthitic K-feldspar phenocrysts (Figs. 2c and 4a). They likely represent former porphyritic granites. Two main facies have been distinguished (migmatite terminology according to Sawyer 2008): (1) metatexitic biotite-rich monzogranitic gneisses in the northern area, characterized by relatively high Fe + Mg + Ti contents and a moderately peraluminous composition; and (2) diatexitic, garnet ± sillimanite-bearing leucogranitic gneisses in the southwest, with low biotite content (Fig. 4a-b) and felsic peraluminous compositions sensu Villaseca *et al.* (1998) (Fig. 5a-b). Compared to the monzogranitic gneiss, the leucogranitic gneisses are also characterized by a more pronounced negative Eu anomaly in their chondrite-normalized REE patterns (Fig. 5c). Moreover, they display anomalous fractionation of the "geochemical twins" Nb-Ta and Zr-Hf, with relatively high Nb/Ta and low Zr/Hf ratios, compared to typical peraluminous granites (Ballouard *et al.* 2016) (Fig. 5f). The sillimanite-bearing and garnet-rich sample ECH23-40 (Fig. 4b) exhibits the highest and even super-chondritic Nb/Ta ratio (>20), and is characterized by a strong depletion in LREE relative to the other orthogneisses, despite nearly identical HREE patterns among the three samples.

Variably deformed, non migmatitic, granitic rocks represent a significant component of the Sioule basement. These include decimeter- to meter-scale (meta)granitoid bodies in the paragneiss or mica schist units (Fig. 2a-b), as well as the granitoid plutons of Chantelle (Fig. 2e) and Saint-Gervais (Fig. 2d).

Among the smaller granitic bodies, ten-centimeter- to several-meter-thick boudins of muscovite granitoids—interlayered within mica schists (ECH22-15a; Fig. 2a) or migmatitic paragneisses (ECH22-43a) of the Sioule series—contain minor biotite and locally sillimanite. These bodies exhibit pervasive and intense solid-state deformation. They are tonalitic to monzogranitic and felsic peraluminous in compositions and exhibit a geochemical signature resembling that of adakite (Moyen, 2009). Their REE patterns show a positive Eu anomaly and significant LREE/HREE fractionation (La/Yb= 21-27) (Fig. 5d), and they are further characterized by Sr enrichment (~200 ppm) and elevated Sr/Y ratios around 60.

The Chantelle biotite granitoids (ECH22-46 and ECH23-30) exhibit a gently dipping foliation marked by stretched biotite and dynamically recrystallized quartz, indicative of incipient sub-solidus deformation (Fig. 4c). They range in composition from granodioritic to monzogranitic and are moderately to highly peraluminous (Fig. 5a-b). Their REE patterns are relatively smooth, *i.e.*, lacking a Eu anomaly. However, the sample ECH22-46, which contains sparse garnet, displays significant enrichment in HREE (Fig. 5d). A meter-scale biotite-bearing monzogranitic body exposed along the Sioule Valley and containing migmatitic paragneiss enclaves (ECH23-41; Figs. 1, 2b and 4d) displays structural, mineralogical, and geochemical characteristics indistinguishable from those of the Chantelle Massif granitoids, and is therefore interpreted as part of the same magmatic lineage.

Two samples of the Saint-Gervais Massif were collected along the Sainte-Christine shear zone where the granite shows C/S fabrics indicative of dextral shear (Fig. 2d). The medium-grained and mesocratic sample ECH23-01 contains biotite fish, tourmaline porphyroclasts, and muscovite aggregates interpreted as cordierite pseudomorphs (Fig. 4e). In contrast, sample ECH23-09 is fine-grained, leucocratic and hosts muscovite fish, along with garnet and tourmaline (Fig. S3e). The two rocks, one highly peraluminous and monzogranitic, and the other felsic peraluminous and leucogranitic, overlap in major element composition with other Saint-Gervais Massif granitoids reported in the literature (Hottin *et al.*, 1989), although literature samples can reach higher Fe + Mg + Ti concentrations (Fig. 5a-b). In contrast to the leucogranite sample showing weak LREE/HREE fractionation and relatively low REE concentrations, the Saint-Gervais monzogranite has a REE pattern similar to the Chantelle monzogranite (Fig. 5d). Overall, granitoids from the Saint-Gervais and Chantelle massifs exhibit a major and trace element compositional range closely resembling that of the archetypal cordierite-bearing peraluminous granitoids of the Guéret Massif (Barbarin, 1996), located west of the Sillon Houiller fault (Cartannaz, 2006).

The Pouzol-Servant porphyritic biotite microgranites (ECH22-16, ECH23-10; Figs. 2f and 4f) as well as the biotite granites of the Champs Massif (ECH22-44; Fig. 2h), including leucocratic facies containing quartz-tourmaline orbicules (ECH22-08; Fig. 2h), do not show evidence for sub-solidus ductile deformation. Except for the Champs orbicular facies, which is more felsic and REE depleted, the Champs and

Pouzol-Servant granites share comparable moderately to highly peraluminous compositions, along with similar Fe + Mg + Ti concentrations and REE patterns (Fig. 5).

One sample of biotite trachy-dacitic tuff from the Manzat Formation (ECH23-27; Fig. S3f), occurring as an enclave within the Champs granite Massif, and two samples of altered (chlorite- and calcite-bearing) trachy-dacitic tuffs from the Châteauneuf Formation, unconformably overlying the paleo-weathered Saint-Gervais granitoid (ECH23-07, 08; Figs. 2g, 4g and S3g), were collected. All samples display a banded texture with aligned feldspar microlites and contain broken crystals, suggesting ash-flow deposition (Fig. 4g). The ignimbritic rocks (and associated lavas reported in the literature) are metaluminous to highly peraluminous, and their major and trace element geochemical signatures, including REE patterns and Nb/Ta and Zr/Hf ratios, appear indistinguishable between the two formations (Fig. 5 and see also Fig. S4 for TAS diagram of volcanic rocks). At the regional scale, those compositions overlap with that of volcanic-sedimentary rocks of the "Tufs Anthracifères series" (Cartannaz, 2006), and the REE patterns of the Sioule ignimbrites closely resemble that of the Pouzol-Servant and Champs (micro)granites (Fig. 5).

The porhyritic granites of the Colettes Massif (ECH22-01, 22-02; Fig. 3e) contain zinnwaldite commonly rimmed by Li-muscovite (see Monnier *et al.*, 2022 for mica compositions), as well as cordierite crystals partially replaced by Li-micas (gigantolite, Fig. 4h). In addition, secondary tourmaline occurs as crack fillings and at mineral grain boundaries. The Colettes granites are generally felsic peraluminous, relatively depleted in LREE with pronounced negative Eu anomaly, and display low Nb/Ta ratios (<5), a characteristic feature of granites genetically associated with hydrothermal Sn and/or W mineralization (Fig. 5) (Ballouard *et al.*, 2016). A rhyolitic dyke sampled south of the Echassières Complex (ECH22-05) contains agglomerates of white and black micas, commonly prismatic in shape, in which relics of cordierite have been observed (Figs. 3e and S3h). This strongly peraluminous and felsic dyke has a similar major element composition to a microgranite found as enclave in the Beauvoir RMG (Raimbault *et al.*, 1995), and exhibits REE patterns nearly identical to the Colettes granite ECH22-02 (Fig. 5e).

4.2 U-Pb geochronology of felsic igneous rocks from the Sioule region

4.2.1 Migmatitic metagranites

Two samples of migmatitic metagranites, one monzogranitic (ECH22-35) and the other leucogranitic (ECH23-18), were selected for zircon U-Pb analyses (see Fig. 6a-b for Tera Wasserburg diagrams and Fig. S5 for Representative CL images of zircon grains). A total of 69 spot analyses were performed on 42 zircon grains from both samples. In ECH22-35, a cluster of five analyses made on four grains, with generally well-defined oscillatory zoning (Fig. S5a) and U contents mostly between ~300 and 600 ppm, yields a concordia date of 495.5 ± 8.3 Ma (MSWD of concordance + equivalence = 1.6). In sample ECH23-18, nine analyses from eight zircon grains exhibiting blurry oscillatory zoning (~200-400 ppm U, Fig. S5b) define a concordia date of 506.6 ± 8.1 Ma (MSWD = 1.8). These dates are interpreted as the crystallization ages of the granitic protoliths. One older concordant analysis from an oscillatory zoned zircon core in sample ECH22-35 with a date of 579 ± 13 Ma (Fig. S5a) is interpreted as inherited. However, younger (sub)concordant analyses that lack distinctive internal textures and scatter along the concordia without forming well-defined age clusters are typically U-rich (>500 ppm; corresponding to relatively high log(α dose) values, *i.e.*, log(α decays.mg^{-1}) >15) and are interpreted as reflecting Pb loss. The remaining discordant analyses most likely result from a combination of Pb loss and common Pb incorporation.

4.2.2 Sioule Series muscovite metagranitoid

Among the 58 analyses on 45 zircon grains from the muscovite metagranitoid (ECH22-15a), deformed in the Sioule Series mica schists, 21 are >90% concordant (Fig. 6c). These include likely inherited grains with Paleoproterozoic to Ordovician dates from 2488 ± 20 to 483 ± 10 Ma, and generally well-defined oscillatory zoning (Fig. S5d). Two concordant analyses of a single grain exhibiting blurry oscillatory zoning along the rim yield a weighted mean $^{206}Pb/^{238}U$ date of 366 ± 7 Ma (MSWD = 0.07). The remaining younger analyses are too discordant to be interpreted reliably and likely experienced Pb loss.

4.2.3 Chantelle and Sioule Series biotite granitoids

Seventy-nine analyses were performed on 48 zircon grains from the Chantelle biotite granitoid (ECH22-46; Fig. 6d). The grains commonly show oscillatory zoning and frequently contain apatite inclusions (Fig. S5c). A cluster of five concordant analyses from four grains yields a concordia date of 607.7 ± 12.7 Ma (MSWD = 1.8), and a single grain gives a date of 491 ± 18 Ma; both are interpreted as inherited. Twelve younger concordant analyses from twelve grains define a concordia date of 353.8 ± 6.4 Ma (MSWD = 1.2), interpreted as the crystallization age of the granitoid. Among the remaining data, one concordant and younger analysis ($^{206}Pb/^{238}U$ age = 326 ± 12 Ma) is enriched in U (1085 ppm, log(α dose) = 15.1), compared to other concordant analyses with ~600-900 ppm and log(α dose) values of 14.9-15.1, and likely reflects Pb loss. The others analyses are significantly discordant due to common Pb incorporation and/or Pb loss.

Several zircon grains from the biotite granitoid containing enclaves of Sioule Series paragneiss (ECH23-41), and geochemically attributed to the Chantelle granitoids (see section 4.1), exhibit resorbed cores rimmed by newly grown zircon (Fig. S5e). Both cores and rims show weakly defined, blurry zoning that is locally oscillatory or patchy. Of the 40 analyses performed on 31 grains, seven (including five rims clearly overgrowing older cores) are subconcordant to discordant, due to variable common Pb incorporation, and define a discordia on a Tera-Wasserburg diagram with a lower intercept date of 339.7 ± 8.0 Ma (MSWD = 1.3; Fig. 6e). Although this discordia yields an initial $^{207}Pb/^{206}Pb_c$ ratio of 0.648 ± 0.086, significantly lower than the model terrestrial value of ~0.86 at 340 Ma (Stacey and Kramers, 1975), anchoring the discordia to this model value increases the

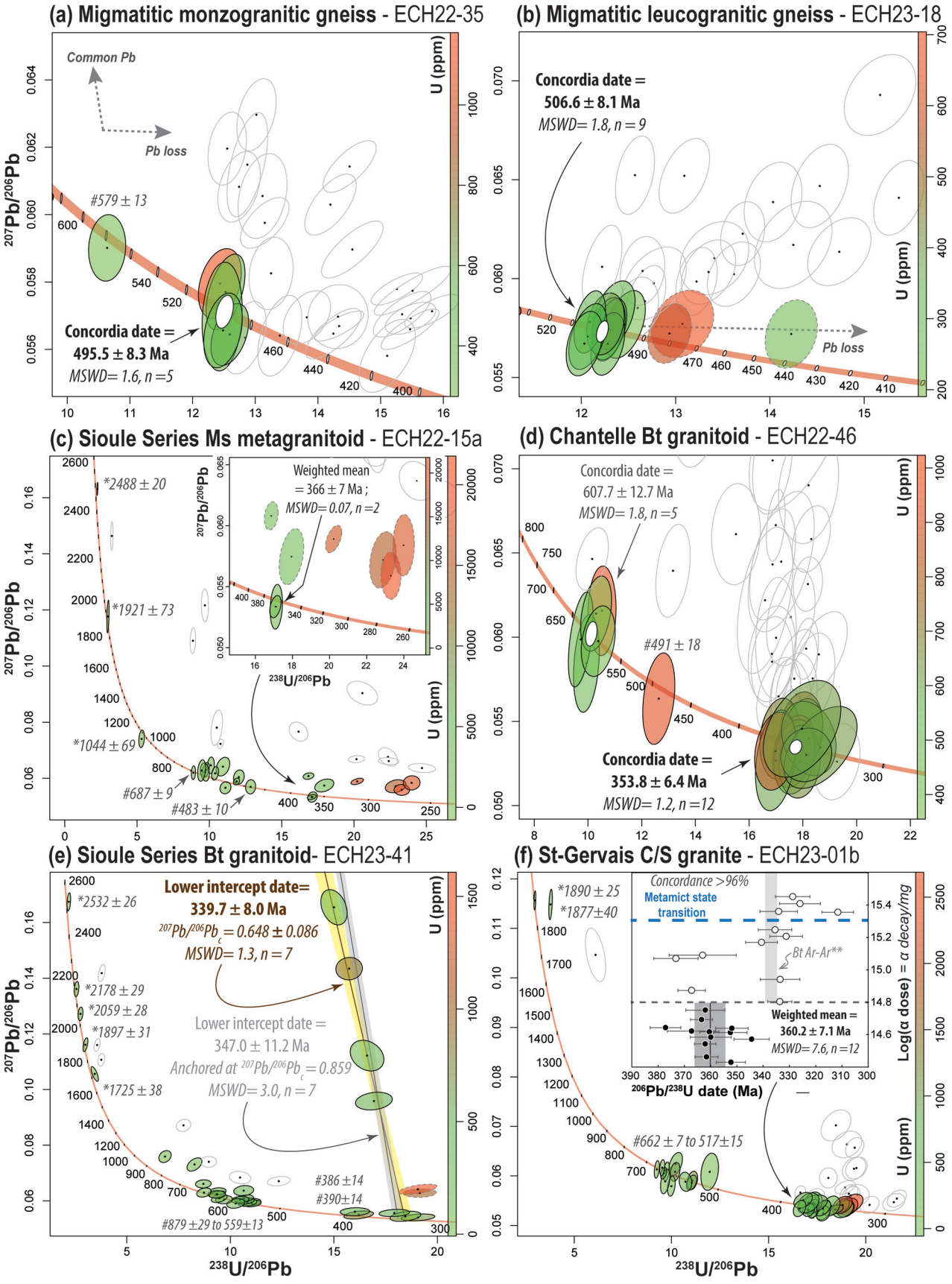
(a) Migmatitic monzogranitic gneiss - ECH22-35
Common Pb
Pb loss
#579 ± 13
Concordia date =
495.5 ± 8.3 Ma
MSWD= 1.6, n =5
(b) Migmatitic leucogranitic gneiss - ECH23-18
Concordia date =
506.6 ± 8.1 Ma
MSWD= 1.8, n = 9
Pb loss
(c) Sioule Series Ms metagranitoid - ECH22-15a
*2488 ± 20
*1921 ± 73
*1044 ± 69
#687 ± 9
#483 ± 10
Weighted mean
= 366 ± 7 Ma ;
MSWD= 0.07, n =2
(d) Chantelle Bt granitoid - ECH22-46
Concordia date =
607.7 ± 12.7 Ma
MSWD= 1.8, n =5
#491 ± 18
Concordia date =
353.8 ± 6.4 Ma
MSWD= 1.2, n =12
(e) Sioule Series Bt granitoid- ECH23-41
Lower intercept date=
339.7 ± 8.0 Ma
207Pb/206Pbc = 0.648 ± 0.086
MSWD= 1.3, n = 7
Lower intercept date =
347.0 ± 11.2 Ma
Anchored at 207Pb/206Pbc = 0.859
MSWD= 3.0, n = 7
*2532 ± 26
*2178 ± 29
*2059 ± 28
*1897 ± 31
*1725 ± 38
#386 ±14
#390±14
#879 ±29 to 559±13
(f) St-Gervais C/S granite - ECH23-01b
*1890 ± 25
*1877±40
Concordance >96%
Metamict state
transition
Bt Ar-Ar**
Weighted mean =
360.2 ± 7.1 Ma
MSWD= 7.6, n =12
#662 ± 7 to 517±15
U (ppm)
207Pb/206Pb
238U/206Pb
206Pb/238U date (Ma)
Log(α dose) = α decay/mg

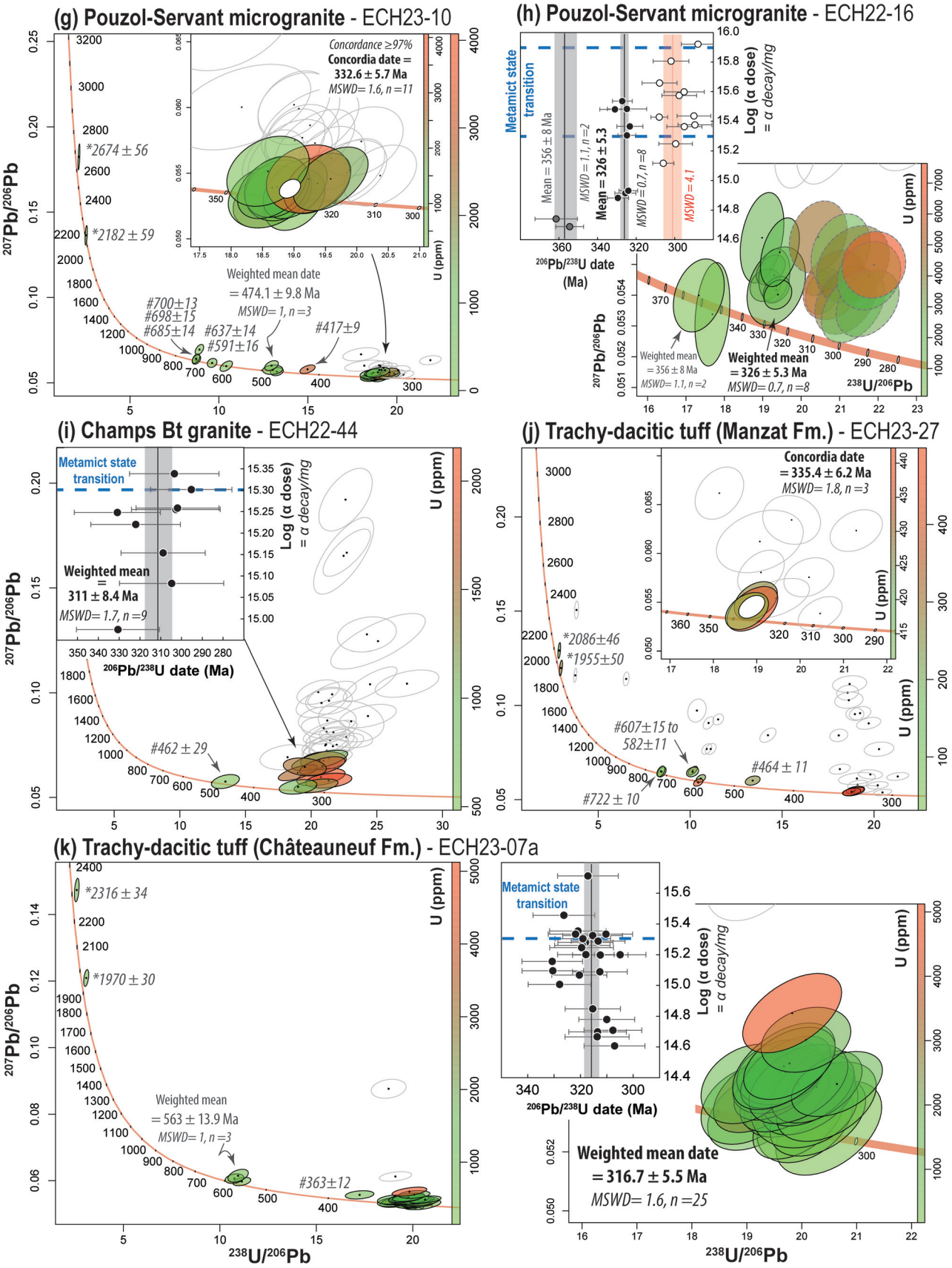
(g) Pouzol-Servant microgranite - ECH23-10
Concordance ≥97%
Concordia date = 332.6 ± 5.7 Ma
MSWD= 1.6, n =11
*2674 ± 56
*2182 ± 59
Weighted mean date = 474.1 ± 9.8 Ma
MSWD= 1, n =3
#700±13
#698±15
#685±14
#637±14
#591±16
#417±9
(h) Pouzol-Servant microgranite - ECH22-16
Metamict state transition
Mean = 356 ± 8 Ma
MSWD = 1.1, n =2
Mean = 326 ± 5.3
MSWD = 0.7, n =8
MSWD = 4.1
Log (α dose) = α decay/mg
U (ppm)
206Pb/238U date (Ma)
Weighted mean = 356 ± 8 Ma
MSWD= 1.1, n =2
Weighted mean = 326 ± 5.3 Ma
MSWD= 0.7, n =8
(i) Champs Bt granite - ECH22-44
Metamict state transition
Weighted mean = 311 ± 8.4 Ma
MSWD= 1.7, n =9
Log (α dose) = α decay/mg
U (ppm)
206Pb/238U date (Ma)
#462 ± 29
(j) Trachy-dacitic tuff (Manzat Fm.) - ECH23-27
Concordia date = 335.4 ± 6.2 Ma
MSWD= 1.8, n =3
*2086±46
*1955±50
#607±15 to 582±11
#464 ± 11
#722 ± 10
U (ppm)
(k) Trachy-dacitic tuff (Châteauneuf Fm.) - ECH23-07a
*2316 ± 34
*1970 ± 30
Weighted mean = 563 ± 13.9 Ma
MSWD= 1, n =3
#363±12
Metamict state transition
Log (α dose) = α decay/mg
U (ppm)
206Pb/238U date (Ma)
Weighted mean date = 316.7 ± 5.5 Ma
MSWD= 1.6, n =25
207Pb/206Pb
238U/206Pb

Fig. 6. Tera-Wasserburg diagrams showing the U-Pb compositions of zircon from felsic (meta-)igneous rocks in the Sioule region. Diagrams displaying alpha dose values (Dröllner *et al.*, 2022) *versus* $^{206}Pb/^{238}U$ dates are presented for samples with sub-concordant and/or non-equivalent zircon data. The range of metamict state transition follows Chakoumakos *et al.* (1987). Ellipses, error bars, and dates are reported at 2σ, and ellipse colors represent semi-quantitative U concentrations. Colorless or dashed ellipses as well as colorless dots, interpreted as reflecting common Pb incorporation and/or radiogenic Pb loss were not used for date calculations. Other indications: * - $^{207}Pb/^{206}Pb$ date, # - $^{206}Pb/^{238}U$ date.

MSWD to 3 (with a lower intercept date of 347.0 ± 11.2 Ma). We therefore interpret the date of 339.7 ± 8.0 Ma as a better estimate for zircon rim crystallization and granitoid body emplacement. Two zircon rims fall to the right of the discordia, and have high U contents (1000-1600 ppm) and log(α dose) values between 15.0 and 15.2 compared to the other analyses (U ~70-900 ppm and log(α dose) = 13.9-15.1). They are interpreted as being affected by Pb loss and excluded from age interpretation. The remaining 24 analyses with concordance >90% define a wide range of inherited dates, from Archean to Neoproterozoic (2532 ± 26 to 559 ± 13 Ma), and even Devonian (390 ± 14 and 386 ± 14 Ma).

4.2.4 Saint-Gervais C/S granite

Zircon grains from the Saint-Gervais C/S monzogranite (ECH23-01b; Figs. 6f and S5f) are commonly fractured, contain unidentified inclusions, and exhibit variably blurred oscillatory zoning. The 53 U-Pb analyses of 41 grains reveal significant inherited component with two Paleoproterozoic dates (1890 ± 25 and 1877 ± 40 Ma), and twelve Neoproterozoic-Cambrian dates between 662 ± 7 and 517 ± 15 Ma generally obtained on grains exhibiting a high, light bluish CL signal. Twenty-six analyses with >96% concordance and $^{206}Pb/^{238}U$ dates between 377 ± 6 and 294 ± 6 Ma scatter along the concordia but do not define a consistent date, suggesting a disturbance of the U-Pb system. Analyses yielding dates younger than 344 ± 7 Ma are characterized by higher U contents and elevated log(α dose) values (14.8-15.5), overlapping the metamictization threshold (15.3-15.9; Chakoumakos *et al.*, 1987), consistent with radiation damage and subsequent Pb loss. In contrast, twelve analyses with log(α dose) <14.8 yield a weighted mean $^{206}Pb/^{238}U$ date of 360.2 ± 7.1 Ma interpreted as the best estimate for zircon crystallization, although the high MSWD of 7.6 indicates some heterogeneity among the data.

4.2.5 Pouzol-Servant biotite microgranite

Two samples from the Pouzol-Servant microgranite were selected for zircon U-Pb dating. Sample ECH23-10 (Fig. 6g) contains numerous inherited zircon grains that generally display high CL signal (Fig. S5h) and yield subconcordant dates spanning the Archean-Paleoproterozoic (2675 ± 56 and 2182 ± 59 Ma), Neoproterozoic (700 ± 13 to 591 ± 16 Ma), and Devonian (417 ± 9 Ma). A cluster of three concordant analyses gives an Ordovician weighted mean $^{206}Pb/^{238}U$ date of 474.1 ± 9.8 Ma (MSWD = 1). Of the 29 further analyses on 20 grains, typically showing an elongated shape, weaker CL signal and blurred oscillatory zoning, the eleven most concordant (≥97%) yield a concordia date of 332.6 ± 5.7 Ma (MSWD = 1.6) interpreted as the age of magma crystallization. Less concordant data likely reflect common Pb incorporation and/or Pb loss. Zircon grains from the second sample, ECH22-16 (Figs. 6h and S5g), show a similar elongated shape with weak CL signal and numerous inclusions. Of the 84 analyses of 37 grains, 63 have a degree of concordance <92%, reflecting disturbance of the U-Pb system. Among the remaining analyses, two concordant spots on a single grain core yield a weighted mean date of 356 ± 8 Ma (MSWD =1.1) interpreted as inherited. Subconcordant data, define two younger date populations. The youngest group comprises non-equivalent analyses of radiation-damaged zircon, characterized by high log(α dose) values between 15.2 and 15.9. In contrast, the second group, returning a weighted mean $^{206}Pb/^{238}U$ date of 326 ± 5.3 Ma (MSWD =0.8), includes zircon with lower dose values (14.9-15.5). This date that is identical within uncertainty with the concordia date obtained on ECH23-10 sample likely reflects the magma crystallization.

4.2.6 Champs biotite granite

In the Champs biotite granite, the only identified inherited component corresponds to a single concordant analysis performed on a zircon core displaying a high CL signal and oscillatory zoning, yielding a date of 462 ± 29 Ma (Figs. 6i and S5k). The other 36 analyses, from 27 grains, are strongly discordant to subconcordant. The grains commonly host apatite inclusions and display relatively weak CL signal with an internal texture ranging from homogeneous to oscillatory zoned. The nine most concordant zircon grains (88-99% concordance) yield a weighted mean $^{206}Pb/^{238}U$ date of 311.0 ± 8.4 Ma (MSWD = 1.7, n=9) interpreted as the age of magma crystallization.

4.2.7 Trachy-dacitic tuffs

Like the Sioule granitoids, the trachy-dacitic tuffs of the Manzat (Fig. 6j; ECH23-27) and Châteuneuf (Fig. 6k; ECH23-07a) formations contain a significant proportion of zircon grains that are likely inherited, and generally characterized by high CL signal (Fig. S5j, S5l). In ECH23-27 sample, the date of these grains (n=5) range from Paleoproterozoic (2086 ± 46 and 1955 ± 50 Ma), through Neoproterozoic (607 ± 15 to 582 ± 11 Ma) to Ordovician (464 ± 11 Ma). In ECH23-07a sample, two Paleoproterozoic grains (2313 ± 34 and 1970 ± 30 Ma), three Neoproterozoic grains (weighted mean $^{206}Pb/^{238}U$ date of 563 ± 14 Ma) and one early-Carboniferous grain (363 ± 12 Ma) have been identified. Three analyses on two grains in sample ECH23-27 showing homogeneous texture and blurred oscillatory zoning yield a concordia date of 335.4 ± 6.2 Ma (MSWD=1.8). In ECH23-07a, a cluster of 25 concordant to sub-concordant analyses (94-100%) from grains with textures ranging from homogeneous, oscillatory zoned to sector zoned yield a weighted mean $^{206}Pb/^{238}U$ date of 316.7 ± 5.5 Ma

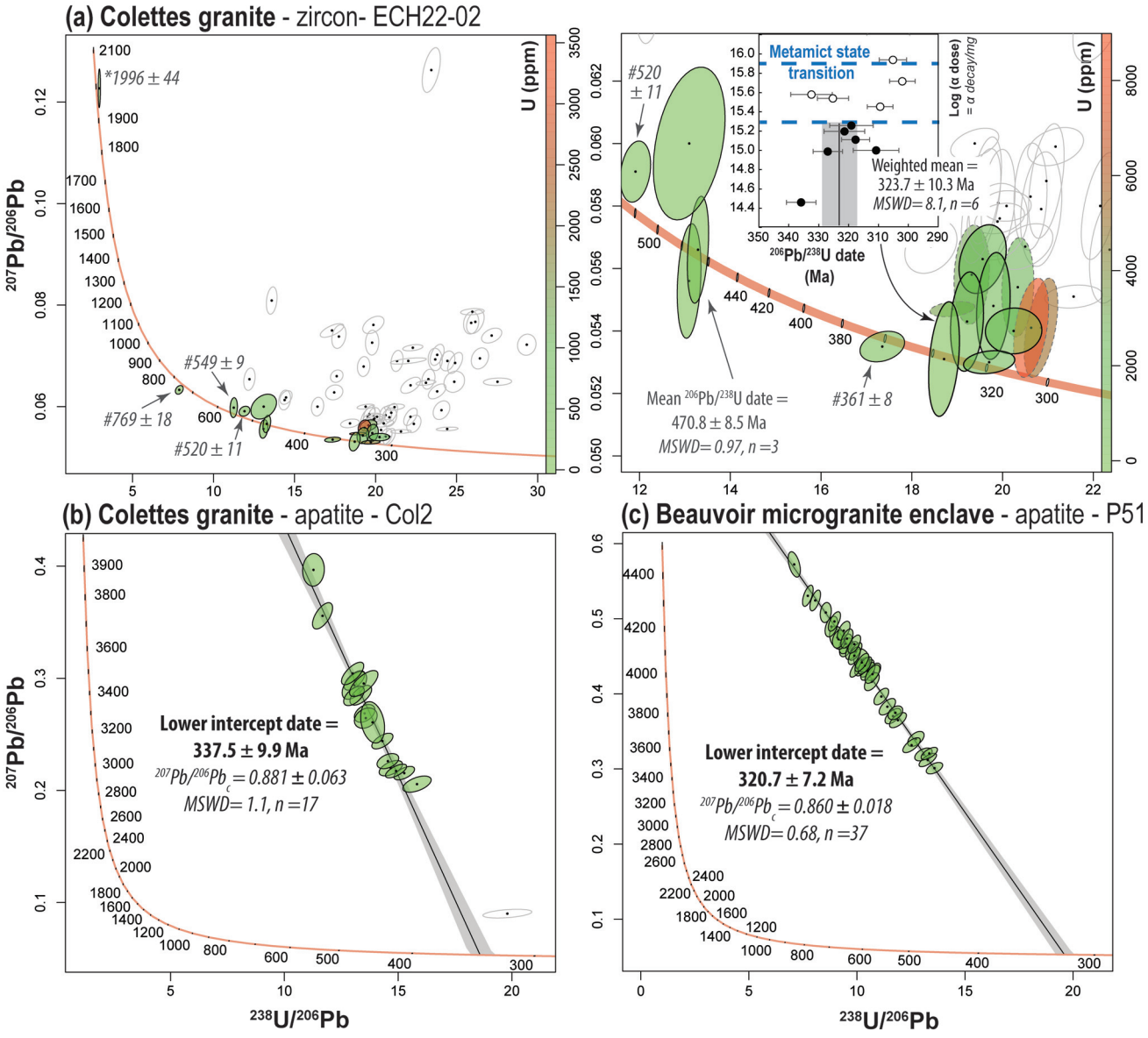

Fig. 7. Tera-Wasserburg diagrams showing the U-Pb compositions of (a) zircon and (b) apatite from the Colettes granites as well as (c) apatite from its microgranite sub-equivalent occurring as an enclave within the Beauvoir RMG. See caption of Figure 6 for additional details on the diagrams and date calculations.

(MSWD = 1.6). Both dates likely record distinct magma crystallization events that shortly preceded eruption. The remaining discordant to sub-concordant analyses (46 in ECH23-27 and two in ECH23-07a) likely reflect post-crystallization disturbance of the zircon U-Pb system.

4.2.8 Colettes granite and Beauvoir microgranite enclave

Seventy two analyses were performed on 44 zircon grains from the Colettes granite sample ECH22-02. The majority (n = 53) are discordant, affected by Pb loss and/or common Pb incorporation, and were excluded from interpretation (Fig. 7a). The remaining subconcordant to concordant analyses derive from zircon grains exhibiting a variety of internal textures, ranging from homogeneous and weakly luminescent to oscillatory zoned (Fig. S5i). Eight sub-concordant analyses from eight grains, including several zircon cores, return dates interpreted as inherited. These include one Paleoproterozoic, two Neoproterozoic, and four Cambrian-Ordovician dates (three of which define a weighted mean $^{206}Pb/^{238}U$ date of 470.8 ± 8.5 Ma; MSWD = 0.97), as well as one early Carboniferous date. Eleven younger analyses scatter along the concordia in concordant to sub-concordant positions, with $^{206}Pb/^{238}U$ dates from 336 ± 5 to 302 ± 4.3 Ma. Excluding radiation-damaged zircon with log(α dose) values between 15.3 and 15.9, yields a weighted mean $^{206}Pb/^{238}U$ date of 323.7 ± 10.3 Ma with significant dispersion (MSWD = 8.1).

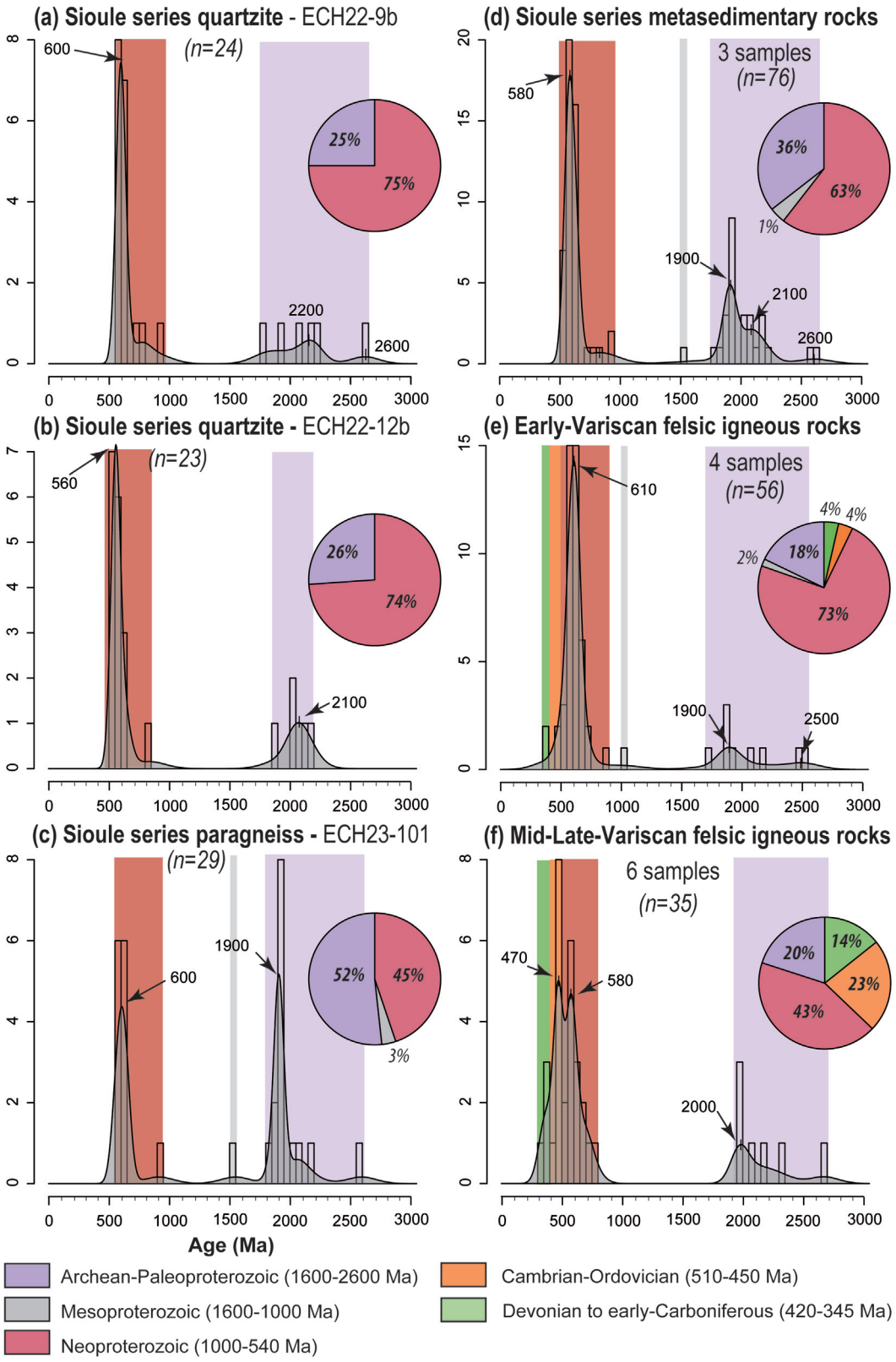

Fig. 8. Histograms, Kernel-density estimates (KDE) and pie charts of U-Pb dates obtained on detrital zircon from metasedimentary rocks of the Sioule Series (a-d) and on inherited zircon from (e) early-Variscan (360-350 Ma) and (f) mid- to late-Variscan (340-310 Ma) felsic igneous rocks from the Sioule region. KDEs and histograms were generated using bandwidths and bin widths of 50 Ma.

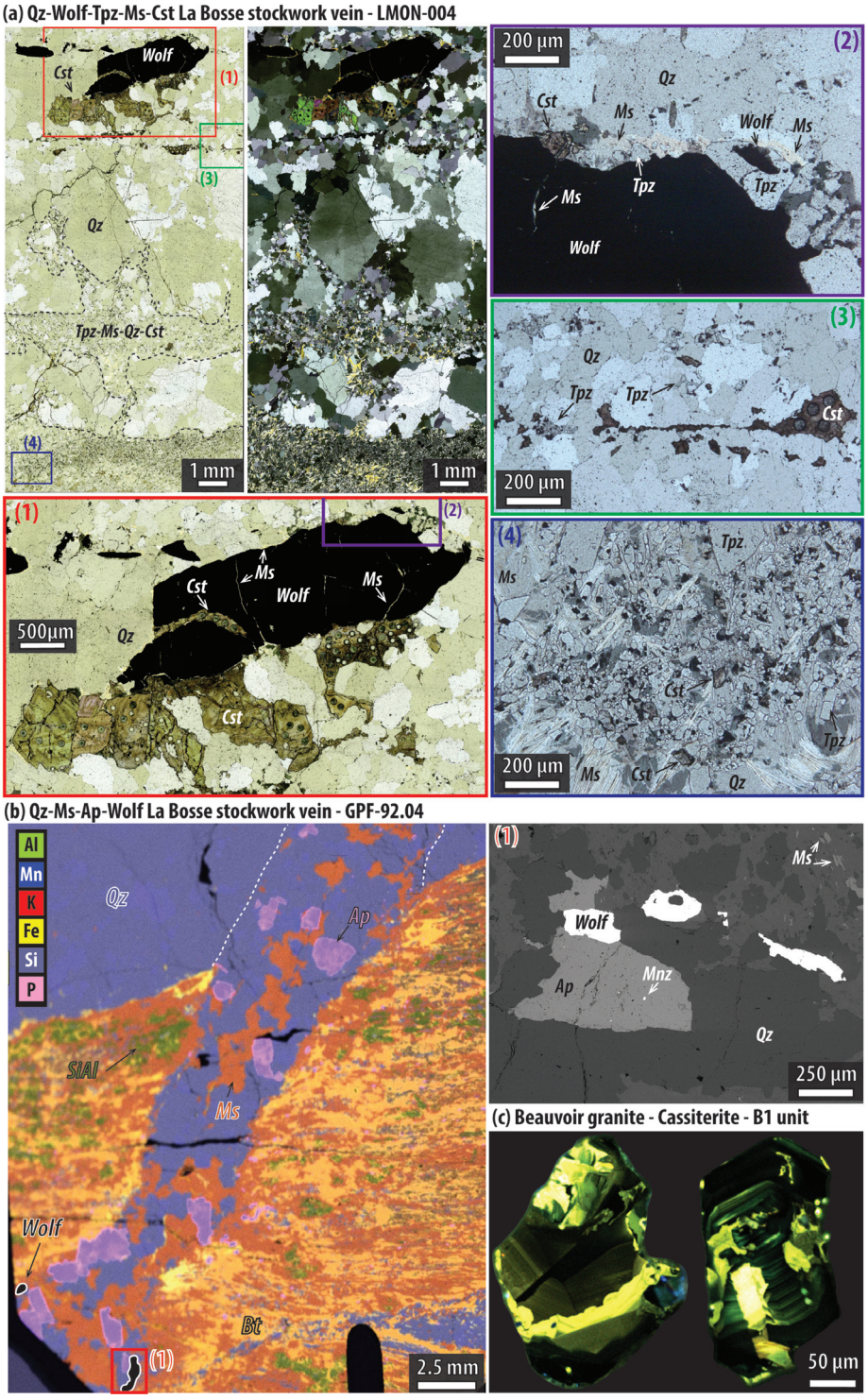

Fig. 9. Petrographic features of dated wolframite, cassiterite and apatite in the Echassières complex. (a) Quartz vein from the La Bosse stockwork (plane-polarized and cross-polarized light), showing wolframite corroded by an assemblage of cassiterite, topaz and muscovite (1-2). Fine-grained topaz, muscovite, cassiterite and quartz occur either as discrete crack-fillings (3) or as larger zones (4) crosscutting or infilling the boundaries of coarser quartz grains showing evidence of dynamic recrystallization (undulose extinction and subgrains). In (1) cassiterite form vein-like infill crosscutting wolframite, and in (3) topaz replaces wolframite along an irregular, embayed contact. In (4), the darker zones correspond to cavities. (b) Micro-XRF chemical map of a quartz-muscovite-apatite-wolframite vein from the La Bosse stockwork crosscutting mica schist and early quartz lens (see Fig. 3d for location of the thin section). Note the spatial relationship between wolframite and apatite. (c) Example of cathodoluminescence (CL) images of cassiterite grains from the B1 unit of the Beauvoir granite showing oscillatory zonation locally truncated by high-CL signal zones.

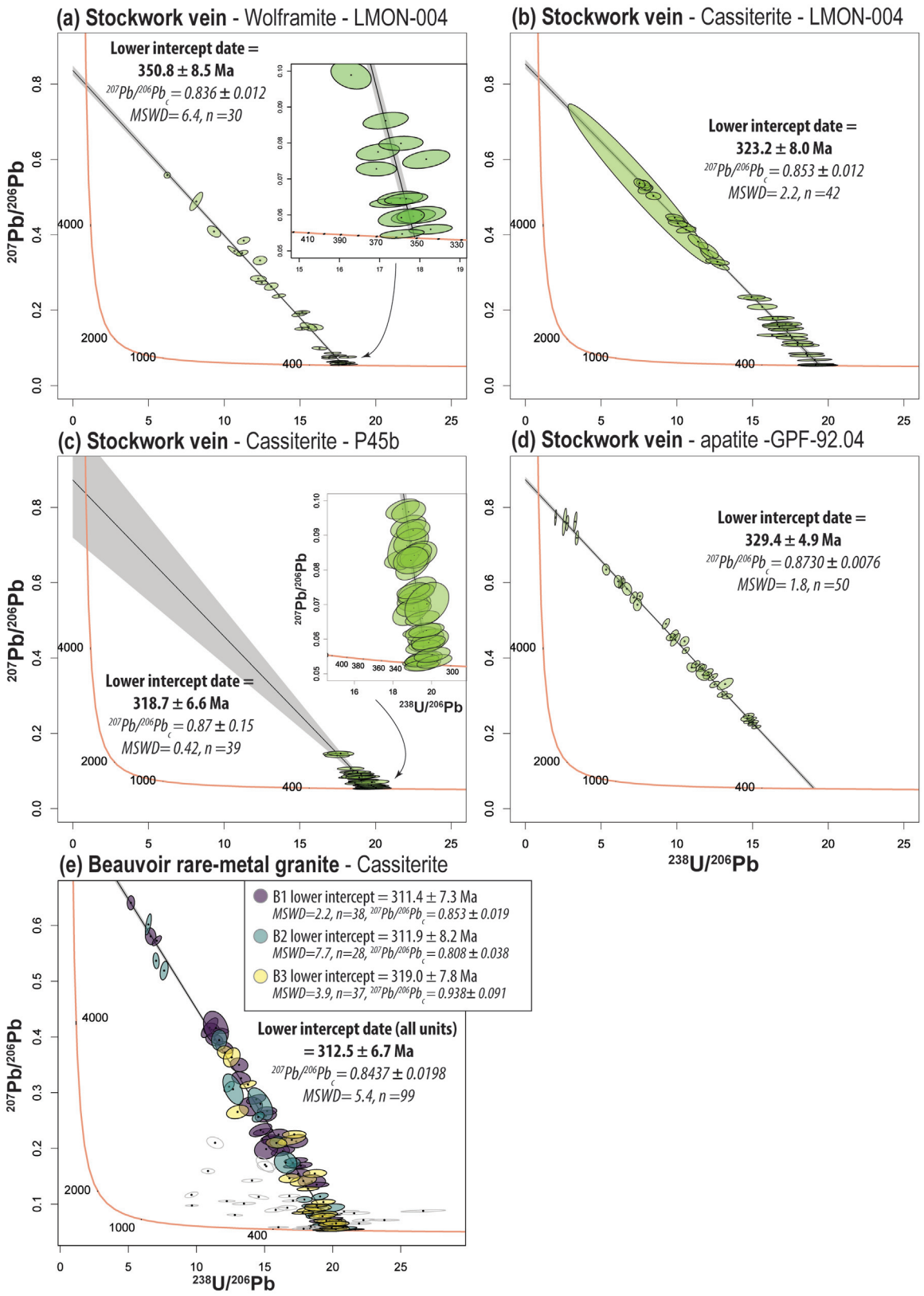

Fig. 10. Tera-Wasserburg diagrams showing the U-Pb compositions of (a), wolframite, (b-c) cassiterite and (d) apatite from distinct veins from the La Bosse stockwork as well as (e) disseminated cassiterite from the Beauvoir rare-metal granite including B1 to B3 units. See caption of Figure 6 for additional details on the diagrams and date calculations.

To better constrain the timing of crystallization of the Colettes granite, apatite U-Pb dating was conducted on sample Col2 (a counterpart of ECH22-01) and on the P51 microgranite enclave, geochemically equivalent to the main Colettes intrusion, hosted within the Beauvoir RMG (Fig. 7b-c). Analyses of subhedral to anhedral apatite grains (see Fig. S6 for representative CL images), variably enriched in common Pb, plot in discordant positions in the Tera-Wasserburg diagram. For Col2, excluding a single younger spot interpreted as affected by Pb loss, the remaining seventeen analyses define a lower intercept date of 337.5 ± 9.9 Ma (MSWD = 1.1) and an initial $^{207}Pb/^{206}Pb_c$ composition of 0.881 ± 0.063 similar to the model terrestrial Pb composition at that time (~0.86). In the microgranite enclave, 37 analyses of euhedral to subhedral apatite grains yield a lower intercept date of 320.7 ± 7.2 Ma (MSWD = 0.68), with a common Pb composition of 0.860 ± 0.018.

4.3 Zircon U-Pb record of Sioule metasedimentary rocks

A total of 117 U-Pb analyses were performed on 87 zircon grains from the three metasedimentary rock samples of the Sioule Series. Of these, we retrieved 76 dates corresponding to individual concordant (>90%) analyses or to weighted mean dates calculated from multiple concordant analyses of individual grain domains. All three samples display two main zircon date populations: an Archean-Paleoproterozoic group (*ca.* 2600-1600 Ma) with peaks at *ca.* 2100 and 1900 Ma, and a Neoproterozoic group (mostly between *ca.* 800 and 540 Ma) with peaks at *ca.* 600 or 560 Ma. Only one grain yielded a Mesoproterozoic date (Fig. 8a-d).

The Neoproterozoic population accounts for ~75% of the detrital zircon component in the quartzite samples ECH22-09b (mica schist unit) and ECH22-12b (paragneiss unit). In contrast, this proportion decreases to ~50% in the paragneiss sample ECH23-101, due to the presence of a significant number of Paleoproterozoic zircon grains (n = 11). These define an upper intercept date of 1929 ± 36 Ma (MSWD = 1.1, n = 13) in a Wetherill concordia diagram, with a lower intercept at 720 ± 198 Ma, consistent with Neoproterozoic Pb loss (Fig. S7). The maximum depositional ages, based on the youngest coherent group of zircon dates, are indistinguishable within analytical uncertainty across the three samples: 571.9 ± 9.4 Ma (weighted mean $^{206}Pb/^{238}U$ date; MSWD = 1.9, n = 6) for ECH22-09b, 553.9 ± 9.9 Ma (weighted mean $^{206}Pb/^{238}U$ date; MSWD = 1.9, n = 6) for ECH22-12b, and 567.2 ± 10.6 Ma (concordia date; MSWD = 2.5, n = 4) for ECH23-101, consistent with an Ediacaran sedimentary protolith (Fig. S7).

4.4 U-Pb geochronology of rare-metal mineralization from the Echassières complex

4.4.1 La Bosse stockwork

The La Bosse stockwork vein sample LMON-004, occurring as a raft within an aplitic dyke, records a multiphase crystallization history. An early coarse-grained assemblage (~500 μm to several millimeters), composed of quartz with plastic deformation features (*i.e.*, undulose extinction and subgrain development), and wolframite, was partially overprinted by a finer-grained assemblage (10s of μm to ~1 mm) including quartz, topaz, muscovite, and cassiterite (Fig. 9a). Cassiterite clearly replaces wolframite, notably as vein-like infill, and occurs as crack-fill within the early quartz. In the Tera-Wasserburg diagram, 30 wolframite analyses plot in sub-concordant to discordant positions (Fig. 10a). Despite a relatively high MSWD of 6.4, the discordia defines a lower intercept date of 350.8 ± 8.5 Ma and $^{207}Pb/^{206}Pb_c$ ratio of 0.836 ± 0.012. 42 concordant to sub-concordant analyses of cassiterite yield a significantly younger intercept date of 323.2 ± 8.0 Ma (MSWD =2.2, $^{207}Pb/^{206}Pb_c$ = 0.853 ± 0.012) (Fig. 10b) that is similar to the date of 318.7 ± 6.6 Ma (n=39, MSWD =0.42, $^{207}Pb/^{206}Pb_c$ = 0.87 ± 0.15) obtained from cassiterite of the stockwork vein sample P45b, occurring in enclave in the B3 unit of the Beauvoir RMG (Fig. 10c).

In the La Bosse stockwork quartz-muscovite vein sample GPF-92.04, millimeter-scale apatite occurs in close association with wolframite crystals up to 300 μm in size (Fig. 9b). The limited quantity of wolframite precluded direct dating but apatite grains that likely co-crystallized with wolframite, yield a lower intercept date of 329.4 ± 4.9 Ma (n=50, MSWD=1.8, $^{207}Pb/^{206}Pb_c$ = 0.873 ± 0.008; Fig. 10d).

4.4.2 Beauvoir rare-metal granite

In the Beauvoir RMG, CL images of mounted cassiterite grains commonly reveal oscillatory zonation locally truncated by high-CL-intensity zones, possibly reflecting hydrothermal overprint (Fig. 9c). Nonetheless, a total of 99 analyses from the B1, B2 and B3 units yield a coherent lower intercept date of 312.5 ± 6.7 Ma (MSWD=5.4, $^{207}Pb/^{206}Pb_c$ = 0.844 ± 0.020; Fig. 10e), in agreement with published crystallization ages of the granite. Individually, cassiterite from the B1, B2 and B3 units yield lower intercept dates indistinguishable within error of 311.4 ± 7.3 Ma (MSWD=2.2, n=38), 311.9 ± 8.2 Ma (MSWD=7.7, n=28) and 319.0 ± 7.8 Ma (MSWD=3.9, n=37), respectively, with the higher degree of statistical dispersion occurring in the deeper B2 and B3 units.

5 Discussion

5.1 Pre-Variscan crustal framework of the Sioule region

Detrital zircon U-Pb analyses of metasedimentary rocks do not distinguish between the signatures of the mica schist and paragneiss units and suggest that their protoliths were deposited at or after 550-570 Ma (see maximum deposition ages in Fig. S7 and in Supplementary Tab. S7). These siliciclastic sediments predominantly originated from the erosion of Neoproterozoic igneous rocks (*ca.* 800-540 Ma) and their sedimentary derivatives, with variable contribution from *ca.* 2600-1600 Ma late-Archean to Paleoproterozoic basement sources (Fig. 8a-d). This zircon record matches that of Ediacaran sediments largely sourced from the erosion of the Cadomian-Avalonian belt (Linnemann *et al.*, 2008; Melleton *et al.*, 2010; Chelle-Michou *et al.*, 2017; Ballouard *et al.*, 2018; Couzinié *et al.*, 2019; Passos Do Carmo *et al.*, 2025), an Andean-type orogen that developed along the active northern margin of Gondwana during the late-Neoproterozoic, and is now exposed, for instance, in the North Armorican Massif

(Fig. 1a) (Ballèvre *et al.*, 2001; Chantraine *et al.*, 2001; Linnemann *et al.*, 2014). The > 1600 Ma zircon grains suggest detrital input from distinct domains of the cratonic hinterland of the Cadomian orogen. Based on previous studies (*e.g.*, Chelle-Michou *et al.*, 2017; Couzinié *et al.*, 2019; Stephan *et al.*, 2019), the zircon component peaking at *ca.* 2200-2100 Ma likely originated from the West African Craton, with possible contributions from Eburnean basement relics in the North Armorican Domain (Poujol *et al.*, 2024), while the 1929 ± 36 Ma population (Fig. S7c) may reflect contributions from the Saharan Metacraton or the Arabian-Nubian Shield. Alternatively, the abundance of *ca.* 1930 Ma zircon grains in the Sioule paragneiss sample ECH23-101 could indicate a proximal, yet unidentified Paleoproterozoic source within the FMC.

During the early-Paleozoic, the metasedimentary rocks or their protoliths were likely intruded by (leuco)granitic magmas, now occurring as migmatitic orthogneisses within the Sioule Series, and dated between 506.6 ± 8.1 and 495.5 ± 8.3 Ma (Fig. 6a-b and Tab. S7). This Cambrian-Ordovician magmatic event, well expressed and documented notably in the European Variscan belt, relates to post-Cadomian extension along the Gondwana margin and predominantly involves the partial melting of Ediacaran metasediments (Melleton *et al.*, 2010; Ballèvre *et al.*, 2012; Tichomirowa *et al.*, 2012; Laurent *et al.*, 2017; Ballouard *et al.*, 2018; Couzinié *et al.*, 2022; García-Arias *et al.*, 2024). In the Sioule region, the occurrence of a *ca.* 580 Ma old inherited zircon in one of the orthogneiss samples (Fig. 6a) along with their peraluminous compositions (Fig. 5b) is consistent with derivation from such metasedimentary sources.

The two identified facies, one monzogranitic and the other leucogranitic, could belong to the same magmatic lineage, the latter being a more evolved equivalent. A comparable relationship between meta-leucogranites (leucogneisses) and meta-porhyritic granites (augen gneisses) has also been proposed for the *ca.* 540 Ma Velay orthogneiss formation in the southeastern FMC (Couzinié *et al.*, 2017). In the Sioule region, this interpretation is notably supported by the more pronounced negative Eu anomaly and lower Zr/Hf ratios of the leucogranitic gneisses, indicative of feldspar and zircon fractionation, respectively (Linnen and Keppler, 2002) (Fig. 5c, f). The higher Nb/Ta ratio of the leucogranitic gneisses is not consistent with such relationship as Nb/Ta should behave similarly as Zr/Hf during fractional crystallization (Linnen and Keppler, 1997). However, given that Nb is preferentially retained in residual biotite during anatexis compared to Ta (Stepanov and Hermann, 2013), we attribute the anomalously high Nb/Ta ratios of the diatexitic leucogranitic gneisses, relative to the metatexitic monzogranitic gneiss, to a higher degree of partial melting. This is in agreement with the higher modal abundance of inferred peritectic garnet and sillimanite in the gneiss ECH23-40, which records the highest Nb/Ta ratio (Figs. 4a-b and 5c). In addition, the strong depletion in LREE in this sample may indicate that the temperature of partial melting was high enough to dissolve monazite, thereby mobilizing these elements into the melt.

The presence of migmatitic Cambrian-Ordovician metagranites, alongside anatectic Ediacaran metasedimentary rocks, at depth in the Sioule region is supported by the significant proportion of 510-450 Ma inherited zircon grains in Variscan peraluminous magmatic rocks. This inherited component is rare in 360-350 Ma, Early Variscan, granitoids but represents about 23% of zircon inheritance from granites and tuffs younger than 340 Ma (Fig. 8e-f). Additionally, five inherited grains (~14%) from these mid- to late-Variscan felsic igneous rocks yielded Devonian to early-Carboniferous ages, between 420 and 350 Ma, also reflecting the magmatic recycling of early-Variscan (meta)granites. As documented in other part of the European Variscan belt such as the FMC (Turpin *et al.*, 1990; Laurent *et al.*, 2017), the Armorican (Ballouard *et al.*, 2018) and Iberian (López-Moro *et al.*, 2017) massifs, the Cambrian-Ordovician orthogneisses, and more locally early-Variscan felsic (meta)igneous rocks, likely represent a significant component of the source region of peraluminous magmas.

5.2 Early-Variscan tectonic-magmatic evolution

The earliest Variscan felsic igneous rocks in the region may be represented by the muscovite-biotite-bearing leucogranitic to leucotonalitic gneisses founded as boudins within the Sioule series (Fig. 2a). The 366 ± 7 Ma date from a single zircon grain in one of these metagranitoids (Fig. 6c), along with the distributed ductile deformation in these rocks, supports an early Variscan emplacement. However, further geochronological analyses are required to constrain their crystallization age, and additional investigations are needed to clarify the significance of their adakitic geochemical signature, notably marked by strong LREE/HREE fractionation and Sr enrichment (Figs. 5 and 11).

The Chantelle granitoid crystallized at 353.8 ± 6.4 Ma (Figs. 6d and 12) from a peraluminous granodioritic to granitic magma (Fig. 5) and shows a weak, low dipping foliation (Figs. 2e and 4c), broadly concordant with that of its host rock consisting of migmatitic paragneisses (Grolier, 1971). A small granitoid body intruding the Sioule Series, with similar deformational, mineralogical, and geochemical features as the Chantelle granitoid, hosts paragneiss enclaves that display a more pronounced, yet concordant, sub-horizontal foliation (Figs. 2b, 4d, 5 and 11). Zircon U-Pb dating of this body yielded an age of 339.7 ± 8.0 Ma, overlapping considering uncertainty with that of the Chantelle granitoid, albeit less precisely constrained (Figs. 6e and 12). The incipient subsolidus deformation affecting these biotite (± garnet) granitoids points to a syn- to late-tectonic emplacement relative to the flat-lying foliation of the Sioule Series gneisses, which mostly developed during Barrovian metamorphism and related nappe tectonics (Feybesse and Teygey, 1987; Schulz *et al.*, 2001; Schulz, 2009). Anatexis in the Sioule Series may have been synchronous with the emplacement of the Chantelle granitoid at *ca.* 355 Ma and predates 340 Ma, as also documented by the U-Pb dating of metamorphic monazite in the Lower Gneiss Unit of the Pontgibaud area, tens of kilometers south of the Sioule region (Passos Do Carmo *et al.*, 2025).

Despite significant disturbance of their U-Pb system, possibly due to deformation and associated hydrothermal activity along the Sainte-Christine shear zone, as recorded by biotite ^{40}Ar-^{39}Ar dates until *ca.* 335 Ma (Faure *et al.*, 2002),

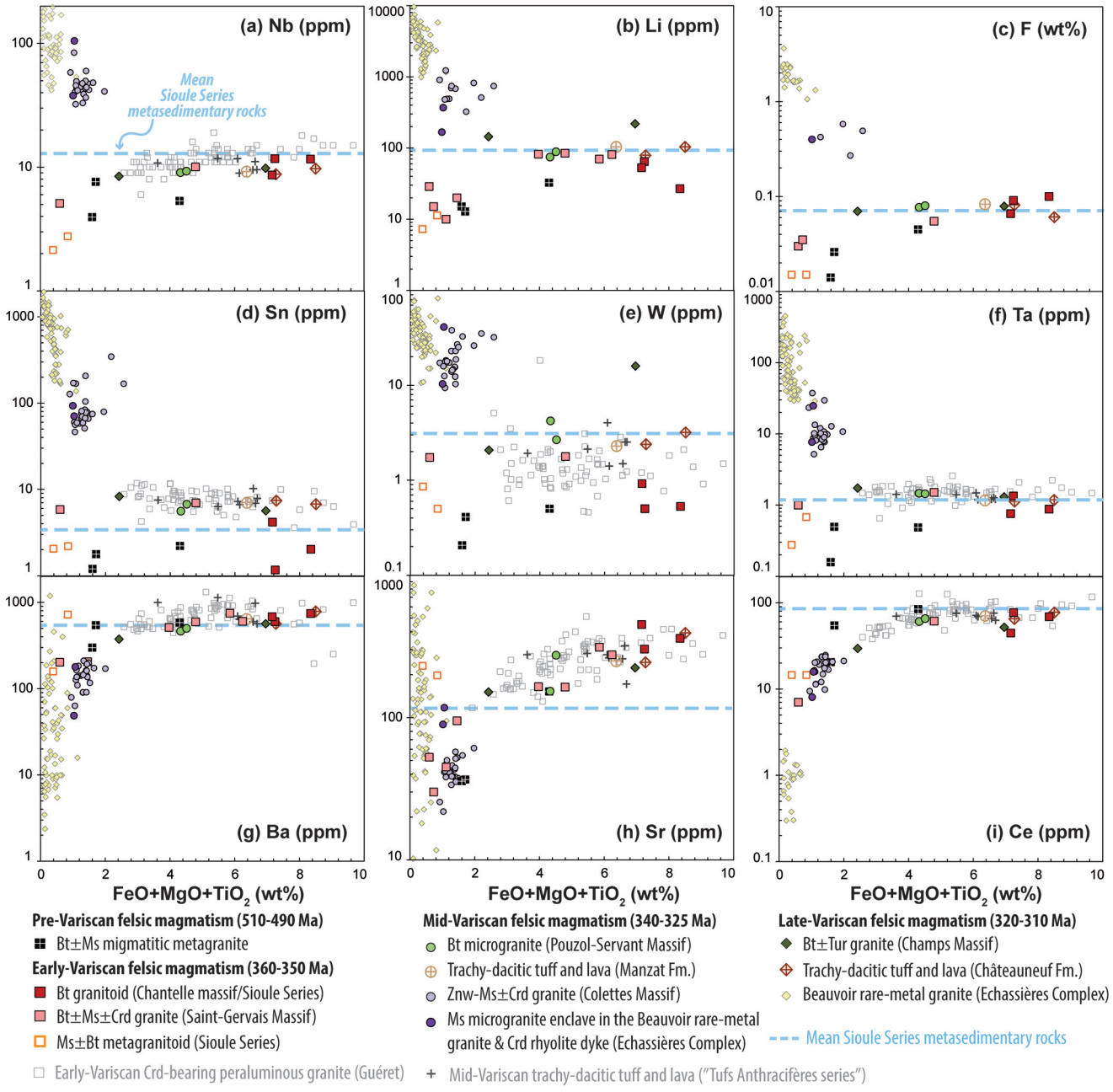

Fig. 11. Evolution of trace element concentrations in felsic (meta-)igneous rocks from the Sioule region as a function of the differentiation index FeO + MgO + TiO_2. For comparison, the composition of early-Variscan cordierite-bearing peraluminous granitoids (CPG) of the Guéret Massif and mid-Variscan trachy-dacitic tuffs and lavas ("Tufs anthracifères" series) are shown (Cartannaz, 2006), in addition to the mean compositions of metasedimentary rocks of the Sioule series (n=13; Rocher *et al.*, 2024).

the least radiation-damaged zircon grains from the Saint-Gervais granite yield a crystallization age of 360.2 ± 7.1 Ma (Figs. 6f and 12). This zircon U-Pb age is similar to that of the Chantelle granitoids and, more broadly, to the emplacement age of the Guéret Massif granitoids on the western side of the Sillon Houiller fault (*ca.* 360-350 Ma; Cartannaz *et al.*, 2007b; Marcoux *et al.*, 2021). Together, the Chantelle granitoids and the Saint-Gervais granite, largely consisting of biotite-cordierite ± muscovite-bearing facies (CPG; Figs. 2d and 4e), with subordinate muscovite ± garnet-bearing varieties (MPG; Fig. S3e), show overlapping major and trace element compositions with the Guéret CPG (Cartannaz, 2006; Cartannaz *et al.*, 2007a) (Figs. 5 and 11), further supporting a comparable origin and timing of crystallization. As well documented in the European Variscan Belt, the C/S granites commonly represent granitic magmas that crystallized during active shearing (Berthé *et al.*, 1979; Gapais, 1989). This suggests that dextral deformation along the Sainte-Christine

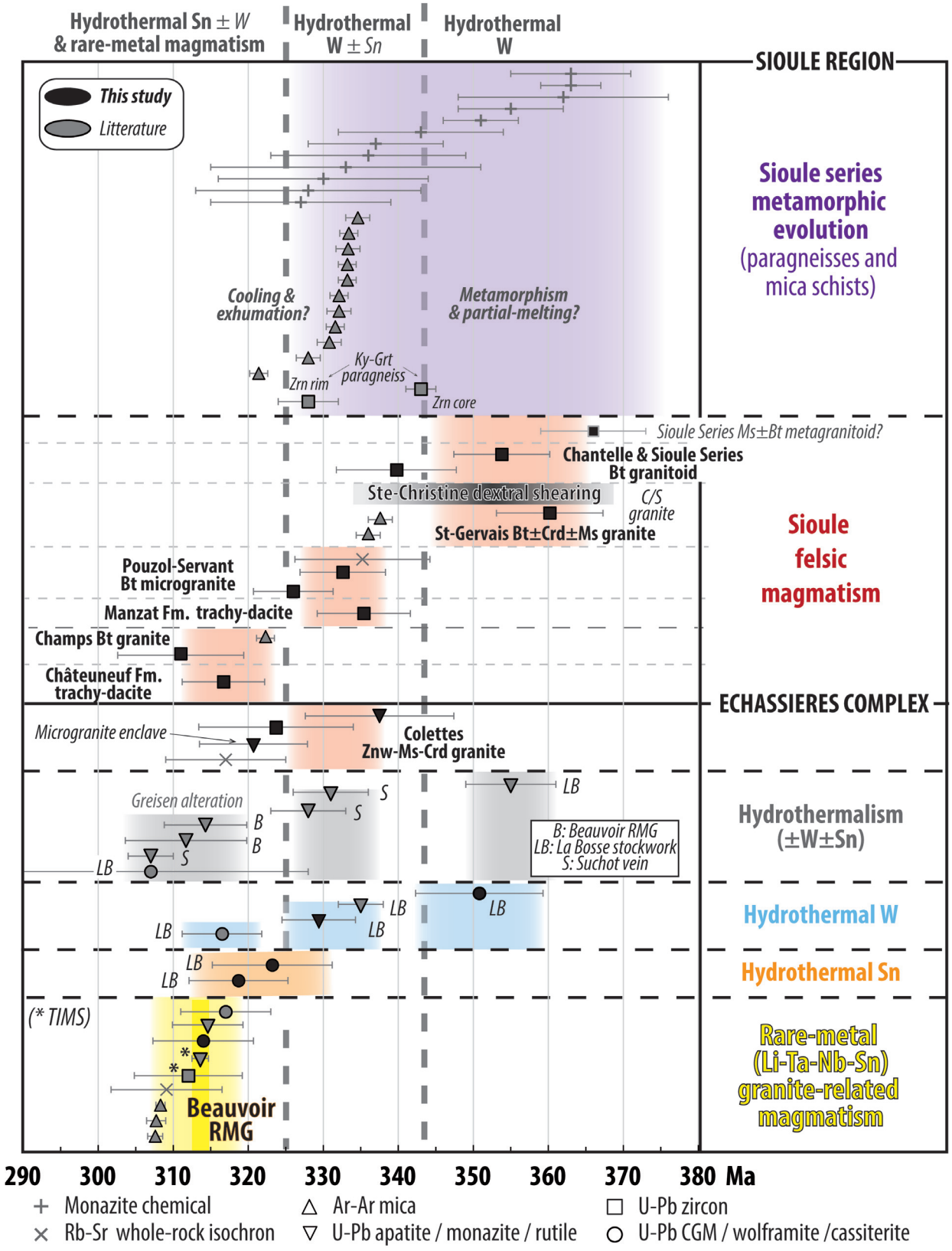

Fig. 12. Compilation of geochronological data from the Sioule region and the Echassières district. Data from this study are shown in black and those from literature are displayed in grey (Duthou and Pin, 1987; Pin, 1991; Cheilletz *et al.*, 1992; Faure *et al.*, 2002; Schulz, 2009; Melleton *et al.*, 2015; Do Couto *et al.*, 2016; Carr *et al.*, 2021; Monnier *et al.*, 2021; Rocher *et al.*, 2024; Esteves *et al.*, 2025a). Rb-Sr isochron ages were recalculated using ^{87}Rb decay constant of Villa *et al.* (2015). See Table S7 for a summary of U–Pb ages obtained in this study.

shear zone was active at *ca.* 360-350 Ma, and possibly persisted until *ca.* 335 Ma, as suggested by biotite ^{40}Ar-^{39}Ar dating (Figs. 12 and 13a). Similarly, dextral transcurrent tectonics along N130-N110-trending vertical faults affecting the Guéret CPG are constrained between *ca.* 360 and 350 Ma in the western FMC (Cartannaz *et al.*, 2007b).

5.3 Mid-Variscan tectonic-magmatic evolution

The Li-mica-cordierite Colettes granite pluton yielded apatite and zircon U-Pb dates of 337.5 ± 9.9 and 323.7 ± 10.3 Ma, respectively, and its microgranitic sub-equivalent, occurring as enclave in the Beauvoir RMG, yielded an apatite U-Pb date of 320.7 ± 7.2 Ma (Fig. 7). While we cannot entirely exclude partial resetting of the apatite U-Pb system in the microgranite enclave during the emplacement of the Beauvoir RMG at *ca.* 313 Ma, the three U-Pb dates overlap at *ca.* 327 Ma. Therefore, we propose 330–325 Ma as the most representative range for the emplacement of the Colettes granite pluton and likely related microgranites (Fig. 12). Considering uncertainty, this range overlaps with the Rb-Sr whole-rock isochron age of the Colettes granite at 317 ± 8 Ma (Pin, 1991; ^{87}Rb decay constant of Villa *et al.*, 2015).

The mid-Variscan period is also marked by the crystallization of the Pouzol-Servant biotite microgranite which yielded zircon U-Pb ages of 332.6 ± 5.7 Ma and 326 ± 5.3 Ma (Fig. 6g-h) similar to the Rb-Sr isochron age of 335 ± 9 Ma (Pin, 1991; Villa *et al.*, 2015). Like the Colettes pluton, this laccolith was emplaced in the Sioule Series mica schists below the transition with the paragneiss unit and lacks evidence of pervasive subsolidus deformation (Grolier, 1971; Faure *et al.*, 1993). However, the rotation of vertical magmatic fabric defined by K-feldspar phenocrysts in the Colettes granite has been interpreted as indicating emplacement within a pull-apart zone controlled by N60-trending sinistral shearing (Jacquot and Gagny, 1985; Gagny and Jacquot, 1987). Moreover, the Pouzol-Servant microgranite is thrust over the Sioule Series paragneisses on its western contact (Grolier, 1971). The structural features of both plutons, together with the presence of N10- to N40-striking extensional quartz veins and granitic dykes around the Echassières complex (Aubert, 1969)—including cordierite rhyolites with a geochemical signature similar to the Colettes granite (Figs. 3e, 5, 11 and S2h)—are compatible with the regional NW-SE extension described by Faure *et al.* (1993) (Fig. 13b).

At *ca.* 335 Ma, N50- to N70-trending volcanic grabens in the northeastern part of the FMC accommodated the deposition of volcanic-sedimentary rocks, including ignimbrites and felsic lavas, of the "Tufs Anthracifères series" (Bertaux *et al.*, 1993). A likely equivalent of this regionally widespread felsic volcanism in the Sioule area is represented by the trachy-dacitic tuffs and lavas of the Manzat Formation, later intruded and thermally metamorphosed by the Champs granite (Fig. 13b-c). Although the concordia age of 335.4 ± 6.2 Ma obtained for a sample from this formation is based on only two zircon grains (Fig. 6j), the plutonic-volcanic connection between the Pouzol-Servant microgranite and those ignimbrites, already suggested by Vennat (1982), is supported by their similar bulk rock composition, notably their REE patterns (Fig. 5).

5.4 Late-Variscan tectonic-magmatic evolution

During the late-Carboniferous, a second plutonic-volcanic event is expressed in the southeastern part of the Sioule region by the intrusion into Visean volcanic-sedimentary rocks of the Champs granitic pluton at *ca.* 320-310 Ma (Faure *et al.*, 2002) (Fig. 6i), and by the eruption of trachy-dacitic tuffs and lavas of the Châteauneuf Formation at 316.7 ± 5.5 Ma (Figs. 6k and 13c). The younger age of the Châteauneuf ignimbrites relative to those of the Manzat Formation is further supported by the higher structural position of the former as shown by topographic profiles at the contact between both units (Fig. S8). In the leucogranitic facies of Champs pluton, the occurrence of quartz-tourmaline orbicules near the contact with the Visean tuffs (Figs. 1, 2h and 13c) suggest low pressure emplacement, as such features indicate boiling of B-rich fluids or the exsolution of hydrous borosilicate melts—processes typical of shallow intrusion roof zones (Samson and Sinclair, 1992; Drivenes *et al.*, 2015).

The bulk-rock compositions of the peraluminous to metaluminous volcanic-sedimentary rocks of the Manzat and Châteauneuf formations, as well as those of the Pouzol-Servant microgranite and the main tourmaline-free facies of the Champs granite, are indistinguishable (Figs. 5 and 11). They also closely resemble other tuffs and lavas assigned to the "Tufs Anthracifères" series occurring on the western side of the Sillon Houiller fault (Cartannaz, 2006; Cartannaz *et al.*, 2007a) (Figs. 5 and 11). The late-Carboniferous age obtained on those ignimbritic rocks during this study is similar to the zircon U-Pb age of 317 ± 2 Ma obtained on one rhyolite of the Montreuilllon region in northeastern FMC (Mercuzot, 2020). Therefore, the new geochronological data indicate that the so-called "Tufs Anthracifères" series encompasses peraluminous to slightly metaluminous felsic volcanic rocks of different ages and should not be considered as a single, regionally time-equivalent marker level at *ca.* 335-330 Ma within the FMC.

In the Echassières complex, the late-Carboniferous period is marked by the emplacement of the Beauvoir RMG at 312.5 ± 6.7 Ma (U-Pb on magmatic cassiterite; Fig. 10e). This age notably aligns with the 313.4 ± 1.3 Ma age obtained *via* CA-ID-TIMS U-Pb dating on apatite (Esteves *et al.*, 2025a). This granite is crosscut by a dense network of NNE-SSW to NE-SW-striking quartz-muscovite veins (related to greisen alteration), also dated at *ca.* 315-310 Ma (Monnier *et al.*, 2021; Rocher *et al.*, 2024). These structures, interpreted as tension gashes, support tectonically controlled magmatic-hydrothermal activity compatible with regional NW-SE extension (Aubert, 1969; Gagny and Jacquot, 1987; Faure *et al.*, 1993) (Fig. 13c).

5.5 Variscan metallogenic odyssey of the Sioule region

Three main mineralizing periods were identified in the Echassières complex, in relationship with regional felsic magmatic episodes (Figs. 12 and 13). At 350.8 ± 8.5 Ma, an early magmatic-hydrothermal event triggered the precipitation of a first generation of wolframite in the La Bosse stockwork (Fig. 10a). This wolframite is partially replaced by cassiterite, topaz, and muscovite (Fig. 9a), and occurs within a vein

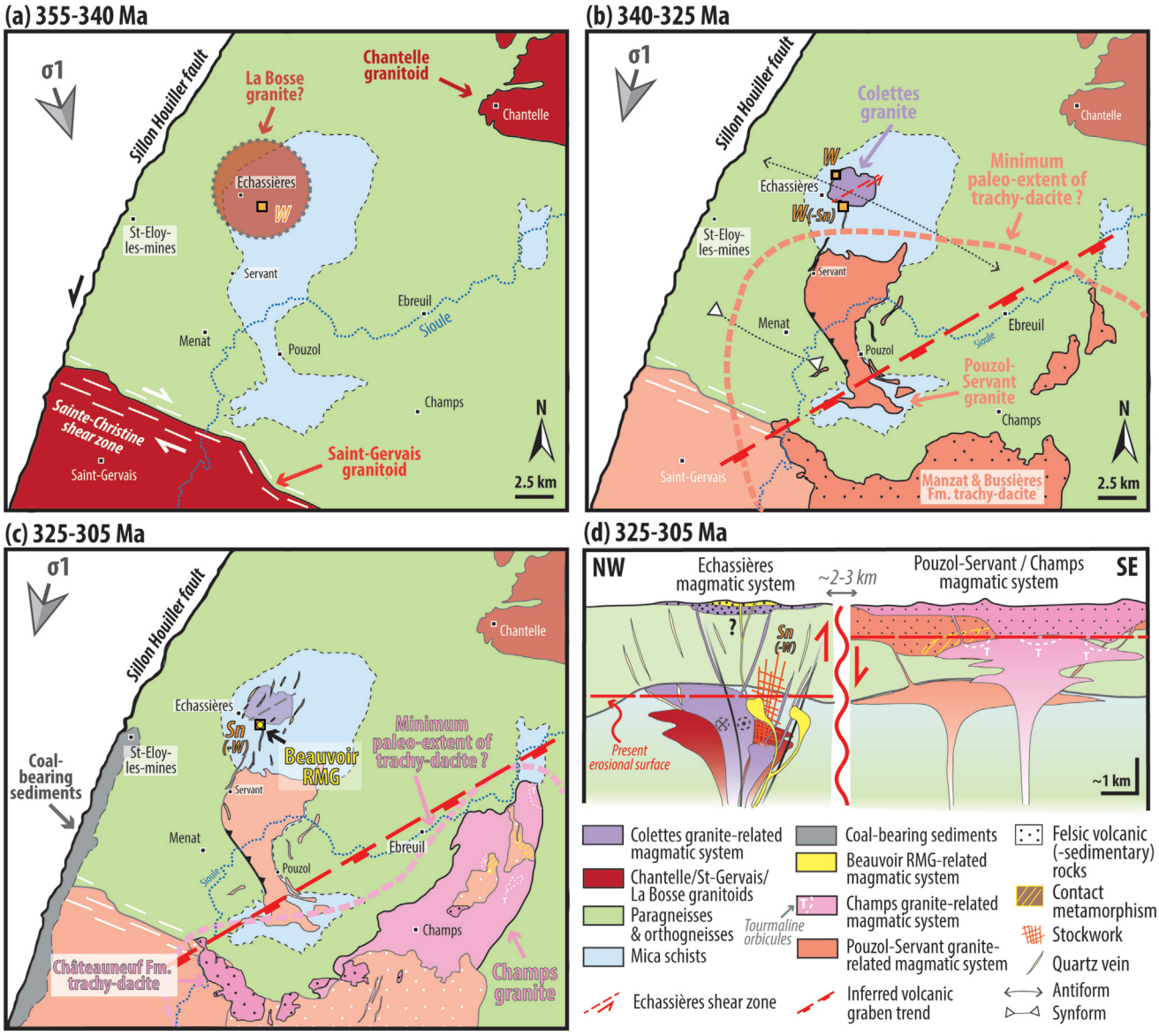

Fig. 13. Schematic illustration of the tectonic-magmatic and metallogenic evolution of the Sioule region from *ca.* 355 to 305 Ma. (a-c) evolutionary geological maps. (d) Conceptual cross sections of the Echassières and Pouzol-Servant /Champs magmatic system at *ca.* 325-305 Ma. In (b-c), the N60-striking thick dashed red line corresponds to the strike of mid-Variscan volcanic grabens in the northeastern FMC (Bertaux *et al.*, 1993), while the sinistral strike-slip shear zone affecting the Colettes granite was documented by Gagny and Jacquot (1987). The main regional shortening directions (σ1) are from Thiery *et al.* (2009).

crosscut by an aplitic dyke (Fig. 3c). This age is consistent with the association of wolframite with coarse-grained quartz exhibiting moderate plastic deformation features, such as undulatory extinction and subgrain development, indicative of brittle-ductile transition conditions (Fig. 9a). Further evidence for this hydrothermal event is provided by a monazite U-Pb date of *ca.* 355 Ma from the alteration halo of stockwork veins (Monnier *et al.*, 2021). This W-rich hydrothermalism was contemporaneous with the emplacement of the Chantelle and Saint-Gervais plutons, which, like the wolframite-bearing quartz vein, generally exhibit only incipient ductile deformation, except along major structural corridors such as the Sainte-Christine shear zone (Fig. 13a).

Like the Guéret CPG to which they are geochemically affiliated, samples from the Chantelle and Saint-Gervais plutons are depleted in F and rare metals (Li, Sn, W, Nb, Ta) compared to Ediacaran metasedimentary rocks of the Sioule Series with a mean W concentration of 3 ppm (Fig. 11). Upon magmatic differentiation—marked by decreasing concentrations of FeO + MgO + TiO_2 and compatible trace elements (Ba, Sr, Ce)—the granitoid rocks evolved toward even lower concentrations of metals and halogens (Fig. 11). Moreover, the high Nb/Ta and Zr/Hf ratios of these early Variscan peraluminous granitoids suggest a limited metallogenic potential for magmatic-hydrothermal deposits (Ballouard *et al.*, 2016). This highlights a major problem regarding the

nature of parental granitic magmas at the origin of this early W mineralization, the inferred La Bosse granite supposedly lying at depth of the eponym stockwork (Cuney and Autran, 1987). Either, early-Carboniferous "rare-metal-fertile" peraluminous granites remain yet to be discovered in the region, or the W mineralization does not stem from a typical orthomagmatic model involving fluids exsolved from a W-rich granitic magma source (Černý *et al.*, 2005) but rather from alternative models involving, for instance, deep metamorphic fluids (Vallance *et al.*, 2001; Cathelineau *et al.*, 2020). Another possibility is that, due to the strong affinity of W for fluids at the magmatic–hydrothermal transition (Schmidt *et al.*, 2020), even weakly evolved peraluminous melts could generate W-rich fluids without extensive differentiation. In this case, the presence of W-rich granites might not be a prerequisite for forming significant mineralization, as suggested by Carr *et al.* (2026) based on geochemical modeling.

Another significant W-mineralizing hydrothermal event likely occurred around 335-330 Ma in the La Bosse stockwork as suggested by the dating of apatite (Fig. 10d) and monazite (Monnier *et al.*, 2021) in textural association with wolframite. This fluid circulation episode was contemporaneous with the emplacement of the Colettes granite at *ca.* 330-325 Ma (Figs. 7 and 13b). In contrast to the contemporaneously emplaced Pouzol-Servant microgranite and associated trachy-dacites which show weak concentrations in W of ~2-4 ppm, the Colettes granite is significantly enriched in rare-metals including W (~10-40 ppm) (Fig. 11). Therefore, this pluton, or its deeper equivalents that fed the rhyolite or microgranite dykes south of the Echassières complex, represents a fertile magmatic source for the stockwork mineralization (Fig. 13d).

The interval from 325 to 310 Ma records one or several metallogenic events, including the precipitation of hydrothermal cassiterite and a third wolframite generation in the La Bosse stockwork, as well as the emplacement of the Beauvoir RMG, which hosts a disseminated magmatic Li, Sn, Nb, Ta ore (Fig. 13c-d). Following its emplacement, the granitic intrusion underwent intense magmatic-hydrothermal alteration involving both magmatic and surface-derived fluids and notably leading to the development of greisen (Merceron *et al.*, 1992; Monnier *et al.*, 2020; Rocher *et al.*, 2024). During this metasomatic process, the W-rich Li-mica lepidolite was locally replaced by W-poor muscovite, generating metal-rich hydrothermal fluids from which the third generation of wolframite in the stockwork likely precipitated (Monnier *et al.*, 2022). This wolframite yielded a U-Pb age of 316.5 ± 5.3 Ma (Carr *et al.*, 2021).

The hydrothermal cassiterite in the La Bosse stockwork precipitated between 323.2 ± 8.0 Ma and 318.7 ± 6.6 Ma (Fig. 10b–c). This timing overlaps with both the emplacement of the Sn-rich Colettes granite (*ca.* 330–325 Ma) and the Beauvoir RMG (*ca.* 313 Ma), preventing the exclusion of either intrusion—or their deep-seated equivalents—as a potential source for the hydrothermal Sn mineralization. Nevertheless, the magmatic fluids exsolved from the Beauvoir RMG magma at *ca.* 313 Ma were strongly enriched in Sn (and likely F) (Harlaux *et al.*, 2017) and were thus capable of precipitating the topaz-cassiterite assemblage observed in the stockwork.

6 Implications and conclusion

The Echassières complex experienced a protracted metallogenic evolution spanning nearly 40 Myr. This evolution is marked by a shift in mineralization styles, from magmatic-hydrothermal W at *ca.* 350 and *ca.* 335-325 Ma, to magmatic-hydrothermal Sn-W and magmatic Li-Sn-Nb-Ta (RMG) at *ca.* 325-310 Ma (Fig. 12). Although the tectonic framework of these mineralizing events is not fully understood, mid-Carboniferous marine transgression (Quenardel *et al.*, 1991) and near-continuous deposition between *ca.* 335-330 and 320-310 Ma of volcanic material in grabens (Bertaux *et al.*, 1993), indicate that extensional tectonics, accompanied by transcurrent deformation (Gagny and Jacquot, 1987), affected the northern part of FMC from *ca.* 335 Ma onward (Fig. 13).

A similar temporal evolution of mineralization types is observed at the scale of the western European Variscan belt (FMC, Iberian Massif, Armorican Massif) when compiling available age data, notably those obtained through U–Pb dating of ore-bearing minerals such as wolframite, cassiterite, and columbite-group minerals (Fig. 14). Sn mineralization events, particularly RMGP emplacement, are confined to the late-Variscan period (320–300 Ma), whereas hydrothermal W deposition occurred throughout the Variscan orogeny (350–300 Ma). In the Saint-Mélany deposit, located in the southern flank of the Velay extensional dome of the FMC, hydrothermal W precipitation at *ca.* 320 Ma preceded Sn mineralization by 4-10 Myr (Harlaux *et al.*, 2023). The mineralized veins were subsequently crosscut by RMG dykes that notably host magmatic cassiterite dated to *ca.* 305 Ma (Harlaux *et al.*, 2023). A temporal decoupling between W (*ca.* 340-305 Ma) and Sn (*ca.* 320–295 Ma) mineralization is also observed in the Iberian Massif, notably the Mortinamor gneiss dome (Bermejo *et al.*, 2025), and the world-class W deposit of Panasqueira, where hydrothermal wolframite (313.8 ± 6.9 Ma) predates hydrothermal cassiterite (297.9 ± 6.1 Ma) (Carr *et al.*, 2026). In the Erzgebirge province of the Variscan Bohemian Massif, polymetallic magmatic-hydrothermal mineralizations also span *ca.* 40 Myr, beginning with W-dominated skarns at *ca.* 338 Ma (Reinhardt *et al.*, 2022). This was followed by a major Sn-W-(Li) mineralization phase in skarn or greisen from *ca.* 327 to 310 Ma, and later by skarn-forming hydrothermal activity with limited metal endowment from 310 to 295 Ma (Zhang *et al.*, 2017; Burisch *et al.*, 2019; Tichomirowa *et al.*, 2019; Reinhardt *et al.*, 2022; Leopardi *et al.*, 2024). At *ca.* 314-312 Ma, RMG of A-type affinity along with associated greisen-type Li-Sn-W deposits were emplaced in transtensional pull-apart basins (Černý *et al.*, 2026).

Generally, the temporal shift from W to Sn mineralizations is attributed to a change in the thermal regime of the underlying crust, with a transition from muscovite- to biotite-breakdown-dominated melting of metasedimentary protoliths, as supported by studies of migmatites and geochemical modeling (Wolf *et al.*, 2018; Zhao *et al.*, 2022a). Additionally, as discussed above, Carr *et al.* (2026) argued that W-rich fluids can be readily produced from weakly evolved (anatectic) melts derived from metapelites without further differentiation, whereas the generation of Sn-rich fluids requires substantial magmatic evolution. This contrast may explain the dominance of W over Sn mineralization during the early stages of the orogeny.

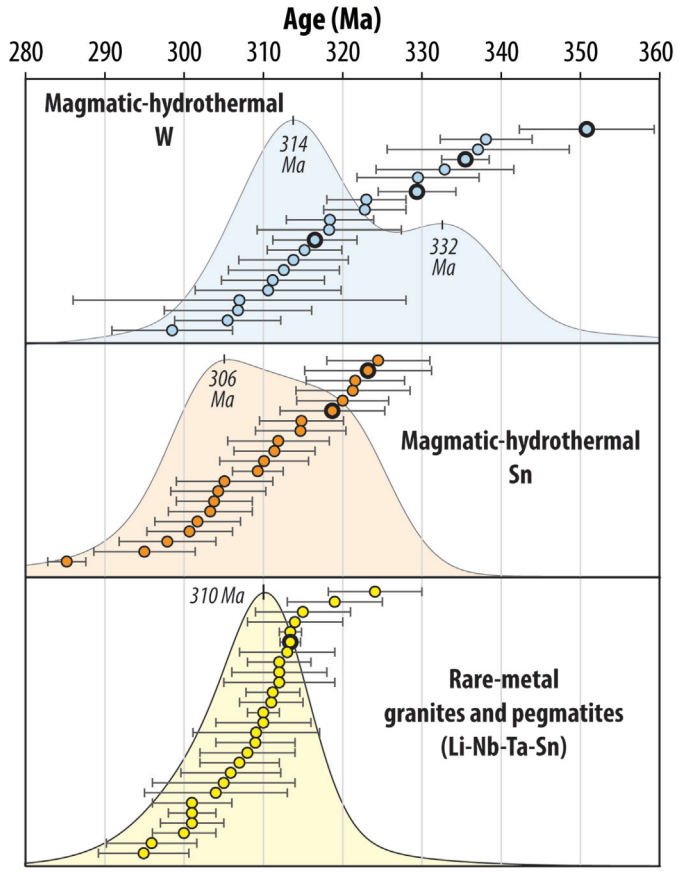

Fig. 14. Compilation of ages and KDE curves for Sn and W magmatic-hydrothermal mineralizing events, and RMGP emplacement, across the western part of the European Variscan belt including the FMC, as well as the Armorican and Iberian massifs. Most data are derived from U–Pb dating of cassiterite, wolframite, and columbite-group minerals. Bold symbols correspond to ages obtained from the Echassières magmatic complex. See Table S10 for data sources and references.

However, these interpretations mainly apply to melts derived from metasedimentary sources, and the change in partial melting conditions of metapelites can hardly account for the late-orogenic nature of RMGPs. Indeed, many elements typically enriched in these granites (Li and W) are expected to be scavenged into the melt at low temperatures during metapelitic anatexis, whereas others (F and Sn) are released near biotite-out conditions (Ballouard *et al.*, 2023). Alternatively, these authors proposed that the formation of RMGPs requires the partial melting of peraluminous metagranites, which can produce anatectic melts enriched in all mica-hosted rare metals due to the breakdown of both muscovite and biotite within a narrow temperature interval. As further suggested by Carr *et al.* (2026), an increasing metafelsic component in the late-orogenic migmatitic crust would naturally result from the upward migration of anatectic fronts and the partial-melting of not only Cambrian-Ordovician orthogneisses but also early-Variscan peraluminous (meta)granites.

In the Echassières complex, the mineralization sequence was accompanied by an increase of the "rare-metal fertility" of peraluminous magmas, from the Colettes granite at *ca.* 330-325 Ma to the Beauvoir RMG at *ca.* 313 Ma (Figs. 5 and 11). In contrast, the Pouzol-Servant and Champs plutonic-volcanic systems, that were broadly contemporaneous with the Echassières granitic magmatism (Figs. 12 and 13), produced rare-metal-depleted felsic magmas, with no apparent increase in magma fertility between the two main pulses at *ca.* 335-330 Ma and *ca.* 320-310 Ma (Figs. 5 and 11).

The localized and protracted intrusion or percolation of "rare-metal-fertile" magmas and fluids in the Echassières complex suggests (1) the presence of a long-lived crustal-scale structure and (2) the existence of a specific deep crustal source capable of generating halogen- and rare-metal-enriched granitic melts. As proposed by Ballouard *et al.* (2023), Koopmans *et al.* (2024), and Carr *et al.* (2026) this source may correspond to peraluminous (meta)granites. In the Sioule region, the inherited zircon record is partly consistent with this hypothesis, as both Cambrian-Ordovician, and possibly Devonian-Early Carboniferous, felsic metaigneous sources were recycled to generate the rare-metal-rich Colettes granite, whose composition approaches that of the Beauvoir RMG.

Acknowledgments

This work was supported by the French National Research Agency through the national program 'Investissements d'avenir' with the reference ANR-10-LABX-21 - RESSOURCES21, the Grand Est region *via* the program 'Jeunes chercheurs' 2020 (19_GE9_066), the ANR TRANSFAIR (ANR-21-CE01-0022-01), the programme TelluS of the Institut National des Sciences de l'Univers, CNRS 2024, and the Imerys company. The LA-ICP-MS laboratory of GeoRessources was funded by the Labex Ressources 21, the Région Lorraine and the European Community through the FEDER program. We are grateful to A. Flammang and J. Moine (GeoRessources lithopreparation platform) for producing the thin and thick sections, to K. Pistre and F. Maubé for assistance with CL imaging, and to L. Salsi and A. Lecomte for their support with micro-XRF and SEM analyses (SCMEM-GeoRessources). We warmly thank the Li-Beauvoir working group at GeoRessources and CRPG, the ANR-TRANSFAIR team, notably C. Gumiaux, as well as the Imerys-EMILI project team, including A. Bargain, B. Barré, G. Jean, and P. Fullenwarth, for the fruitful discussions. We thank O. Vanderhaeghe for editorial handling as well as one anonymous reviewer and M. Burisch for their constructive comments, which significantly improved the manuscript. Finally, this work is dedicated to the memory of Éric Gloaguen, who left us far too soon.

Supplementary material

Fig. S1. Summary of U-Pb ages (2σ) obtained on zircon control materials during the different LA-ICP-MS analytical sessions using the Agilent 8900 (green) and Nu Instruments AttoM ES (red) systems at GeoRessources. The zircon primary reference material was changed from 91500 (Wiedenbeck et al., 1995) in 2023 (a–b) to RAK-17 (Webb et al., 2020) in 2024 (c–d). The recommended age of Temora-2 (Black et al., 2004), RAK-17, Peng-16 (G-Chron3) and 91500 are shown in blue, while calculated mean U-Pb ages are shown in grey. The excess variance in U-Pb ages determined across all

analytical sessions ranges from 0.6% for 91500 (d) to 1.5% for Temora-2 (a).

Fig. S2. Interpretative cross section of the Beauvoir rare-metal granite of the Echassières complex (Cuney et al., 1992; Rocher et al., 2024) showing location of analyzed samples.

Fig. S3. Supplementary photographs of samples from the Sioule region investigated during this study. (a-b) Metasedimentary rock samples collected for detrital zircon U-Pb geochronology within the paragneiss unit: (a) Quartzite interlayered with migmatitic paragneiss; (b) biotite-sillimanite paragneiss. (c-d) Cambrian metatexitic monzogranitic gneiss and diatexitic leucogranitic gneiss. (e) Fine-grained leucogranite from the Saint-Gervais Massif deformed along the Sainte-Christine shear zone. (f) Trachy-dacitic tuff from the Manzat Formation. (g) Trachy-dacitic tuff from the Châteauneuf Formation. (h) Microphotograph of a cordierite crystal almost entirely replaced by white and black micas in the devitrified matrix of a rhyolitic dyke from the Echassières Complex.

Fig. S4. Total alkaki versus silica diagram for (a) (meta-) plutonic rocks (Wilson, 1989) and (b) volcanic rocks (Le Bas et al., 1986) from the Sioule region. Abbreviations: Fm. - Formation.

Fig. S5. Representative cathodoluminescence images of zircon grains from Sioule (meta)igneous rocks. Locations of LA–ICP–MS analytical spots are shown, along with their corresponding analysis numbers and associated 206Pb/238U dates (or 207Pb/206Pb dates for purple analyses). Date uncertainties are reported at the 2σ level.

Fig. S6. Representative cathodoluminescence images of apatite grains from the Colettes granites and Beauvoir microgranite enclave that were analyzed for their U-Pb isotopic compositions.

Fig. S7. U–Pb compositions of detrital zircon grains from metasedimentary rocks of the mica schist (a) and paragneiss (b–c) units of the Sioule Series. Inset diagrams show either 206Pb/238U date distributions (a–b) or a zoomed-in Tera-Wasserburg plot (c) highlighting the youngest detrital zircon dates and corresponding maximum depositional ages. Diagram (1) in panel (c) displays a close-up of the main Paleoproterozoic zircon population identified in sample ECH23-101, along with calculated intercept dates in a Wetherill concordia plot. Ellipses, error bars, and dates are reported at 2σ. Empty ellipses correspond to analyses with a degree of concordance $< 90\%$ and were excluded from the histogram and KDE diagrams in Fig. 8.

Fig. S8. Topographic profiles across the transition between the volcanic-sedimentary rocks of the Châteauneuf and Manzat Formations, constructed using Google Earth and 1:50,000 BRGM geological maps (Hottin et al., 1989). The profiles consistently show the Châteauneuf Formation overlying the Manzat Formation, supporting the interpretation of an older age for the latter.

Supplementary Table 1. Metadata for LA-ICP-MS U–Pb isotopic (and trace element) analyses..

Supplementary Table 2. U–Pb LA-ICP-MS data for apatite, cassiterite, and wolframite control reference materials. Analyses shown in grey were not taken into account in age calculations.

Supplementary Table 3. U–Pb LA-ICP-MS data for apatite, cassiterite, and wolframite samples. Analyses shown in grey were not taken into account in age calculations.

Supplementary Table 4. U–Pb (and trace elements) LA-ICP-MS data for zircon (and glass) control reference materials. Analyses shown in grey were not taken into account in age calculations. LOD = limit of detection.

Supplementary Table 5. Synthesis of U–Pb ages calculated from zircon control reference materials (uncertainties quoted without long-term uncertainty propagation). The data point in grey was rejected from the excess variance calculation.

Supplementary Table 6. U–Pb (and trace elements) LA-ICP-MS data for zircon (and glass) samples. Analyses shown in grey were not taken into account in age calculations.

Supplementary Table 7. Summary of U–Pb geochronological data obtained in this study.

Supplementary Table 8. Whole-rock geochemical data and GPS coordinates of samples from this study. bdl = below detection limit.

Supplementary Table 9. Whole-rock geochemical data compiled from the literature.

Supplementary Table 10. Compilation of ages for Sn and W magmatic-hydrothermal mineralizing events, as well as peraluminous RMG and RMP emplacement, across the west-European Variscan belt including the French Massif central, and the Armorican and Iberian massifs.

The Supplementary Material is available at https://www.bsgf.fr/10.1051/bsgf/2026003/olm.

References

Aïssa M, Marignac C, Weisbrod A. 1987a. Le stockwerk à ferbérite d'Echassières: évolution spatiale et temporelle; cristallochimie des ferbérites. *Géologie la Fr*: 311–333.

Aïssa M, Weisbrod A, Marignac C. 1987b. Caractéristiques chimiques et thermodynamiques des circulations hydrothermales du site d'Echassières. *Géologie la Fr*: 335–350.

Alsac C, D'Arcy D, Souiller R, Féraud J, Giot D, Jeambrun M. 1988. Carte géol. France (1/50000), feuille d'Aigueperse (669), Orléans: BRGM.

Aubert G. 1969. Les coupoles granitiques de Montebras et d'Échassières (Massif Central français) et la genèse de leurs minéralisations en étain, lithium, tungstène et béryllium. *Mémoires du BRGM* 46.

Audren C, Feybesse JL, Tegyey M, Triboulet C. 1987. Relations entre déformations et cristallisations et chemins PTtd des micaschistes polyphasés d'Echassières. Modèle d'évolution géodynamique. *Géologie la Fr* 43–45.

Ballèvre M, Fourcade S, Capdevila R, Peucat JJ, Cocherie A, Fanning CM. 2012. Geochronology and geochemistry of Ordovician felsic volcanism in the Southern Armorican Massif (Variscan belt, France): Implications for the breakup of Gondwana. *Gondwana Res* 21: 1019–1036.

Ballèvre M, Le Goff E, Hébert R. 2001. The tectonothermal evolution of the Cadomian belt of northern Brittany, France: A Neoproterozoic volcanic arc. *Tectonophysics* 331: 19–43.

Ballouard C, Poujol M, Boulvais P, Branquet Y, Tartèse R, Vigneresse JL. 2016. Nb-Ta fractionation in peraluminous granites: A marker of the magmatic-hydrothermal transition. *Geology* 44: 231–234.

Ballouard C, Poujol M, Zeh A. 2018. Multiple crust reworking in the French Armorican Variscan belt: implication for the genesis of uranium-fertile leucogranites. *Int J Earth Sci* 107: 2317–2336.

Ballouard C, Couzinié S, Bouilhol P, Harlaux M, Mercadier J, Montel JM. 2023. A felsic meta-igneous source for Li-F-rich peraluminous granites: insights from the Variscan Velay dome (French Massif Central) and implications for rare-metal magmatism. *Contrib to Mineral Petrol* 178: 75.

Barbarin B. 1996. Genesis of the two main types of peraluminous granitoids. *Geology* 24: 295.

Barbarin B. 1999. A review of the relationships between granitoid types, their origins and their geodynamic environments. *Lithos* 46: 605–626.

Barbarin B, Belin JM. 1982. The "Saint-Gervais-L'Hérmitage"Hercynian Ductile Shear Zone (French Massif Central). *Comptes Rendu l'académie des Sci. Paris Série II* 294: 1377–1380.

Berger J, Beau-Hurdebourcq L, Serrano J, Benoit M, Grégoire M, Benmammar A, *et al*. 2024. Short-lived active margin magmatism preceding Variscan collision in the Western French Massif Central. *BSGF - Earth Sci Bull* 195: 7.

Bermejo D, Ortega L, Barrios Sánchez S, Tavazzani L, Castiñeiras P, Chelle-Michou C, *et al*. 2025. Late Variscan tectonic orogenic collapse as a trigger for Sn-W mineralizing systems. U-Pb ore geochronology across the Martinamor gneissic dome (Salamanca, Spain). *Ore Geol Rev* 184: 106762.

Bernard-Griffiths J, Gebauer D, Grunenfelder M, Piboule M. 1985. The tonalite belt of Limousin (French Central Massif); U-Pb zircon ages and geotectonic implications. *Bull la Société géologique Fr* 1: 523–529.

Bertaux J., Becq-Giraudon J.-F., Jacquemin H. 1993. Les bassins anthracifères de la Région de Roanne (Loire, Massif central), marqueurs d'une tectonique active durant le Viséen supérieur. *Géologie la Fr* 3–10.

Berthé D, Choukroune P, Jegouzo P. 1979. Orthogneiss, mylonite and non coaxial deformation of granites: the example of the South Armorican Shear Zone. *J Struct Geol* 1: 31–42.

Borrajo I, Tornos F, Stein H, Hanchar JM. 2024. Geochronology and decoupling controls of Sn-(Ta-Li) and W-(Sn) mineralization in the Iberian Variscan Massif, Spain and Portugal. *Ore Geol Rev* 173: 106253.

Breiter K, Förster HJ, Seltmann R. 1999. Variscan silicic magmatism and related tin-tungsten mineralization in the Erzgebirge-Slavkovský les metallogenic province. *Miner Depos* 34: 505–521.

Breiter K, Ďurišová J, Hrstka T, *et al*. 2017. Assessment of magmatic *vs*. metasomatic processes in rare-metal granites: A case study of the Cínovec/Zinnwald Sn–W–Li deposit, Central Europe. *Lithos* 292–293: 198–217.

Bruguier O, Becq-Giraudon JF, Bosch D, Lancelot JR. 1998. Late Visean hidden basins in the internal zones of the Variscan belt: U-Pb zircon evidence from the French Massif Central. *Geology* 26: 627–630.

Burisch M, Gerdes A, Meinert LD, Albert R, Seifert T, Gutzmer J. 2019. The essence of time–fertile skarn formation in the Variscan Orogenic Belt. *Earth Planet Sci Lett* 519: 165–170.

Burisch M, Leopardi D, Guilcher M, Dittrich T, Lehmann B. 2025. Greisen-Hosted Lithium Resources of the Erzgebirge/Krušné Hory Province (Germany and Czech Republic). *Econ Geol* 120: 627–647.

Carr PA, Mercadier J, Harlaux M, *et al*. 2021. U/Pb geochronology of wolframite by LA-ICP-MS; mineralogical constraints, analytical procedures, data interpretation, and comparison with ID-TIMS. *Chem Geol* 584: 120511.

Carr PA, Ballouard C, Marignac C, Cathelineau M, Noronha F, Michaud JAS, *et al*. 2026. Collisional orogen dynamics controls the type, timing and location of critical metal deposits. *Terra Nov* 38: 27–35.

Cartannaz C. 2006. Magmatismes et déformations polyphasés: exemple des massifs de Guéret et de Millevaches (Massif central français): origine des magmas et contexte de mise en place. PhD Thesis, Univ Franche-Comté, France, 317 p.

Cartannaz C, Rolin P, Cocherie A, Henry P, Rossy M. 2007a. Carte géol. France (1/50 000), feuille Aubusson (667). Orléans: BRGM.

Cartannaz C, Rolin P, Cocherie A, Marquer D, Legendre O, Fanning CM, *et al*. 2007b. Characterization of wrench tectonics from dating of syn- to post-magmatism in the north-western French Massif Central. *Int J. Earth Sci* 96: 271–287.

Cathelineau M, Boiron MC, Marignac C, Dour M, Dejean M, Carocci E, *et al*. 2020. High pressure and temperatures during the early stages of tungsten deposition at Panasqueira revealed by fluid inclusions in topaz. *Ore Geol Rev* 126: 103741.

Černý P, Blevin PL, Cuney M, London D. 2005. Granite-Related Ore Deposits. Society of Economic Geologists, Inc. 100th Anniv Vol

Černý P, Ercit TS. 2005. The classification of granitic pegmatites revisited. *Can Mineral* 43: 2005–2026.

Černý J, Thiele ST, Guilcher M, Burisch M, Lehmann U, Kaufmann H, *et al*. 2026. Tectonic controls on lithium deposits in the Erzgebirge/Krušné hory region: Regional scale reconstruction of structural controls on late-Variscan mineralization. *Earth-Science Rev* 274: 105395.

Chakoumakos BC, Murakami T, Lumpkin GR, Ewing RC. 1987. Alpha-decay—Induced fracturing in zircon: The transition from the crystalline to the metamict state. *Science* 236: 1556–1559.

Chantraine J, Egal E, Thiéblemont D, Le Goff E, Guerrot C, Ballèvre M, *et al*. 2001. The Cadomian active margin (North Armorican Massif, France): a segment of the north Atlantic Panafrican belt. *Tectonophysics* 331: 1–18.

Chauris L, Marcoux E. 1994. Metallogeny of the Armorican massif. In *Pre-Mesozoic geology in France and related areas*. Springer Berlin Heidelberg: 243–264.

Cheilletz A, Archibald DA, Cuney M, Charoy B. 1992. Ages $^{40}Ar/^{39}Ar$ du leucogranite à topaze-lépidolite de Beauvoir et des pegmatites sodolithiques de Chédeville (Nord du Massif Central, France). Signification pétrologique et géodynamique. *Comptes rendus l'Académie des Sci Série 2, Mécanique, Phys Chim Sci l'univers, Sci la Terre* 315: 329–336.

Chelle-Michou C, Laurent O, Moyen JF, *et al*. 2017. Pre-Cadomian to late-Variscan odyssey of the eastern Massif Central, France: Formation of the West European crust in a nutshell. *Gondwana Res* 46: 170–190.

Cochelin B, Den Y, Saspiturry N. 2025. West European Variscan Belt dismantling and early fragmentation of Pangea: The key role of the Paleotethys subduction. *Earth-Science Rev* 271: 105304.

Couzinié S, Laurent O, Moyen JF, Zeh A, Bouilhol P, Villaros A. 2016. Post-collisional magmatism: Crustal growth not identified by zircon Hf–O isotopes. *Earth Planet Sci Lett* 456: 182–195.

Couzinié S, Laurent O, Poujol M, Mintrone M, Chelle-Michou C, Moyen JF, *et al*. 2017. Cadomian S-type granites as basement rocks of the Variscan belt (Massif Central, France): Implications for the crustal evolution of the north Gondwana margin. *Lithos* 286–287: 16–34.

Couzinié S, Laurent O, Chelle-Michou C, Bouilhol P, Paquette JL, Gannoun AM, *et al*. 2019. Detrital zircon U–Pb–Hf systematics of Ediacaran metasediments from the French Massif Central: Consequences for the crustal evolution of the north Gondwana margin. *Precambrian Res.* 324: 269–284.

Couzinié S, Laurent O. 2021. Zircon U-Pb dating of the Montredon-Labessonnié orthogneiss by LA-ICP-MS: new evidence for late Ediacaran crustal melting in the French Massif Central. *Géol Fr* 1: 24–31.

Couzinié S, Bouilhol P, Laurent O, Grocolas T, Montel JM. 2022. Cambro–Ordovician ferrosilicic magmatism along the northern Gondwana margin: constraints from the Cézarenque–Joyeuse gneiss complex (French Massif Central). *BSGF - Earth Sci Bull* 193: 15.

Cuney M, Autran A. 1987. Objectifs géneraux du projet GPF Echassières n°1 et resultats essentiels acquis par le forage de 900 m sur le granite albitique à topaze-lepidolite de Beauvoir. *Géologie la Fr* 7–24.

Cuney M, Barbey P. 2014. Uranium, rare metals, and granulite-facies metamorphism. *Geosci Front* 5: 729–745.

Cuney M, Marignac C, Weisbrod A. 1992. The Beauvoir topaz-lepidolite albite granite (Massif Central, France); the disseminated magmatic Sn-Li-Ta-Nb-Be mineralization. *Econ Geol* 87: 1766–1794.

Cuney M, Alexandrov P, Le Carlier De Veslud C, Cheilletz A, Raimbault L, Ruffet G, *et al*. 2002. The timing of W-Sn-rare metals mineral deposit formation in the Western Variscan chain in their orogenic setting: the case of the Limousin area (Massif Central, France). *Geol Soc London, Spec Publ* 204: 213–228.

de Hoÿm de Marien L, Pitra P, Poujol M, Cogné N, Cagnard F, Le Bayon B. 2023. Complex geochronological record of an emblematic Variscan eclogite (Haut-Allier, French Massif Central). *J Metamorph Geol* 41: 967–995.

Debon F, Le Fort P. 1988. A cationic classification of common plutonic rocks and their magmatic associations: principles, method, applications. *Bull Minéralogie* 111: 493–510.

Do Couto D, Faure M, Augier R, Cocherie A, Rossi P, Li XH, *et al*. 2016. Monazite U-Th-Pb EPMA and zircon U-Pb SIMS chronological constraints on the tectonic, metamorphic, and thermal events in the inner part of the Variscan orogen, example from the Sioule series, French Massif Central. *Int J Earth Sci* 105: 557–579.

Drivenes K, Larsen RB, Müller A, Sørensen BE, Wiedenbeck M, Raanes MP. 2015. Late-magmatic immiscibility during batholith formation: assessment of B isotopes and trace elements in tourmaline from the Land's End granite, SW England. *Contrib to Mineral Petrol* 169: 56.

Dröllner M, Barham M, Kirkland CL. 2022. Gaining from loss: Detrital zircon source-normalized α-dose discriminates first-*versus* multi-cycle grain histories. *Earth Planet Sci Lett* 579: 117346.

Duthou JL, Pin C. 1987. Etude isotopique Rb-Sr de l'apex granitique d'Echassières (Granite des Colettes, granite de Beauvoir). *Géologie la Fr*: 63–67.

Esteves N, Bouilhol P, Schaltegger U, Ovtcharova M, Paul AN, France L. 2025a. The magmatic-hydrothermal transition record in zircon: Implications for zircon texture, composition and rare-metal granite dating (Beauvoir granite, French Massif Central). *Eur J Mineral* 37: 667–693.

Esteves N, France L, Cuney M, Bouilhol P. 2025b. Small pluton construction through sills stacking, amalgamation and differentiation: Insight from the Beauvoir granite (Massif Central, France). *Earth ArXiv* preprint. https://doi.org/10.31223/X5KT5V

Faure M, Grolier J, Pons J. 1993. Extensional ductile tectonics of the Sioule metamorphic series (Variscan French Massif Central). *Geol Rundschau* 82: 461–474.

Faure M, Lardeaux JM, Ledru P. 2009. A review of the pre-Permian geology of the Variscan French Massif Central. *Comptes Rendus - Geosci* 341: 202–213.

Faure M, Monié P, Pin C, Maluski H, Leloix C. 2002. Late Visean thermal event in the Northern part of the French Massif Central: New $^{40}Ar/^{39}Ar$ and Rb-Sr isotopic constraints on the Hercynian syn-orogenic extension. *Int J Earth Sci* 91: 53–75.

Feybesse JL, Teygey M. 1987. Evolution tectonométamorphique dévonienne et carbonifère de la série de Sioule (Massif Central français). *Géologie la Fr*: 33–41.

Gagny C, Jacquot T. 1987. Contribution de la pétrologie structurale à la connaissance des conditions de mise en place et de structuration complexe du granite des Colettes (Massif d'Echassières, Massif Central Français). *Géologie la Fr*: 47–56.

Gapais D. 1989. Shear structures within deformed granites: Mechanical and thermal indicators. *Geology* 17: 1144–1147.

García-Arias M, Morales Cámera MM, Dahlquist JA, Gao P, Couzinié S, Díez-Montes A. 2024. The tectonic significance of peri-Gondwanan Late Neoproterozoic-Early Palaeozoic felsic peraluminous magmatism. *Earth-Science Rev* 254: 104803

Gardiner NJ., Palin RM, Koopmans L, Mangler MF, Robb LJ. 2024. On tin and lithium granite systems: A crustal evolution perspective. *Earth-Science Rev* 258: 104947.

Gébelin A, Brunel M, Monié P, Faure M, Arnaud N. 2007. Transpressional tectonics and Carboniferous magmatism in the Limousin, Massif Central, France: Structural and $^{40}Ar/^{39}Ar$ investigations. *Tectonics* 26: 1–27.

Gébelin A, Roger F, Brunel M. 2009. Syntectonic crustal melting and high-grade metamorphism in a transpressional regime, Variscan Massif Central, France. *Tectonophysics* 477: 229–243.

Gourcerol B, Gloaguen E, Melleton J, Tuduri J, Galiegue X. 2019. Re-assessing the European lithium resource potential – A review of hard-rock resources and metallogeny. *Ore Geol Rev* 109: 494–519.

Gourcerol B, Guttierez T, Pochon A, Picault M, Gloaguen E, Fournier E. 2021. Évolution Base de données « Gisements France » : Atlas des substances critiques et stratégiques. BRGM/RP-71133-FR, 66 p.

Grolier J. 1971. Contribution à l'étude géologique des séries cristallophyliennes inverses du Massif Central français: La série de la Sioule, Puy-de-Dôme, Allier. *Mémoire du BRGM* 64.

Harlaux M, Marignac C, Cuney M, Mercadier J, Magott R, Mouthier B. 2015. Nb-Ti-Y-HREE-W-U oxide minerals with uncommon compositions associated with the Tungsten Mineralization in the Puy-Les-Vignes deposit (Massif Central, France): Evidence for rare-metal mobilization by late hydrothermal fluids with a peralkaline signature. *Can Mineral* 53: 653–672.

Harlaux M, Mercadier J, Bonzi WME, Kremer V, Marignac C, Cuney M. 2017. Geochemical signature of magmatic-hydrothermal fluids exsolved from the Beauvoir Rare-Metal Granite (Massif Central, France): insights from LA-ICPMS analysis of primary fluid inclusions. *Geofluids* 2017: 1925817.

Harlaux M, Romer RL, Mercadier J, Morlot C, Marignac C, Cuney M. 2018. 40 Ma years of hydrothermal W mineralization during the Variscan orogenic evolution of the French Massif Central revealed by U-Pb dating of wolframite. *Miner Depos* 53: 21–51.

Harlaux M, Marignac C, Mercadier J, *et al*. 2021. Multistage development of a hydrothermal W deposit during the Variscan late-orogenic evolution: The Puy-les-Vignes breccia pipe (Massif Central, France). *BSGF - Earth Sci Bull* 192: 33.

Harlaux M, Marignac C, Carr PA, *et al*. 2023. Polyphase W-Sn mineralization and rare metal magmatism in relation to the late - Variscan tectono - metamorphic evolution of the southeastern French Massif Central. *Miner Depos* 59 : 47–68

Harlaux M, Blein O, Ballouard C, Kontak DJ, Thiéblemont D, Dabosville A, *et al*. 2025. Geochemical footprints of peraluminous rare-metal granites and pegmatites in the northern French Massif Central and implications for exploration targeting. *Ore Geol Rev* 176: 106409.

Horányi B, Gion AM, Gaillard F, *et al*. 2025. Experimental constraints on the sources of lithium-rich granites and pegmatites. *Commun Earth Environ* 6: 966.

Hottin AM, Belin J, Bois J, Deyrieux G, Morice E, Périchaud JJ, *et al*. 1989. Carte géol France (1/50000), feuille Saint-Gervais-d'Auvergne (668). Orléans: BRGM.

Hottin AM, Gros Y, Marteau P, Marchand G, Maurin G, Debacque G, *et al*. 1991. Carte géol France (1/50000), feuille d'Evaux-les-Bains (643). Orléans: BRGM.

Hulsbosch N. 2019. Nb-Ta-Sn-W distribution in granite-related ore systems: Fractionation mechanisms and examples from the Karagwe-Ankole Belt of Central Africa. *Ore Deposits: Origin, Exploration, and Exploitation*: 75–107.

Hulsbosch N, Boiron MC, Dewaele S, Muchez P. 2016. Fluid fractionation of tungsten during granite-pegmatite differentiation and the metal source of peribatholitic W quartz veins: Evidence from the Karagwe-Ankole Belt (Rwanda). *Geochim Cosmochim Acta* 175: 299–318.

Huston DL, Doublier MP, Eglington B, Pehrsson S, Piercey S, Mercier-Langevin P. 2023. Convergent margin metallogenic cycles: A window to secular changes in Earth's tectonic evolution. *Earth-Science Rev* 245: 104551.

Jacquot T, Gagny C. 1985. Pétrologie structurale du massif d'Echassières (Massif Central français): mise en évidence de l'activité de linéaments lors de sa genèse. *Documents-BRGM*: 39–53.

Joly A, Chen Y, Faure M, Martelet G. 2007. A multidisciplinary study of a syntectonic pluton close to a major lithospheric-scale fault - Relationships between the Montmarault granitic massif and the Sillon Houiller Fault in the Variscan French Massif Central: 1. Geochronology, mineral fabrics, and tectonic implications. *J Geophys Res Solid Earth* 112: 1–18.

Joly A, Martelet G, Chen Y, Faure M. 2008. A multidisciplinary study of a syntectonic pluton close to a major lithospheric-scale fault - Relationships between the Montmarault granitic massif and the Sillon Houiller Fault in the Variscan French Massif Central: 2. Gravity, aeromagnetic investigations, and 3-D geologic modeling. *J Geophys Res Solid Earth* 113: 1–13.

Koopmans L, Martins T, Linnen R, Gardiner NJ, Breasley CM, Palin RM, *et al*. 2024. The formation of lithium-rich pegmatites through multi-stage melting. *Geology* 52: 7–11.

Laurent O, Couzinié S, Zeh A, Vanderhaeghe O, Moyen JF, Villaros A, *et al*. 2017. Protracted, coeval crust and mantle melting during Variscan late-orogenic evolution: U–Pb dating in the eastern French Massif Central. *Int J Earth Sci* 106: 421–451.

Laurent O, Couzinié S, Doucet LS. 2023. Timescales of ultra-high temperature metamorphism and crustal differentiation: Zircon petrochronology from granulite xenoliths of the Variscan French Massif Central. *Earth Planet Sci Lett* 611: 118133.

Ledru P, Lardaux JM, Santallier D, *et al.* 1989. Où sont les nappes dans le Massif central français? *Bull la Société Géologique Fr*: 605–618.

Lehmann B. 2021. Formation of tin ore deposits: A reassessment. *Lithos* 402–403: 105756.

Leopardi D, Gerdes A, Albert R, Gutzmer J, Lehmann B, Burisch M. 2024. LA-ICP-MS U-Pb cassiterite age data of the Sadisdorf deposit link Sn-Li-(W-Cu) mineralization in the eastern Erzgebirge to the collapse of the Altenberg-Teplice Caldera. *Geochemistry* 84: 126038.

Linnemann U, Gerdes A, Hofmann M, Marko L. 2014. The Cadomian Orogen: Neoproterozoic to Early Cambrian crustal growth and orogenic zoning along the periphery of the West African Craton—Constraints from U–Pb zircon ages and Hf isotopes. *Precambrian Res* 244: 236–278.

Linnemann U, Pereira MF, Jeffries TE, Drost K, Gerdes A. 2008. The Cadomian Orogeny and the opening of the Rheic Ocean: The diacrony of geotectonic processes constrained by LA-ICP-MS U-Pb zircon dating (Ossa-Morena and Saxo-Thuringian Zones, Iberian and Bohemian Massifs). *Tectonophysics* 461: 21–43.

Linnen RL, Keppler H. 1997. Columbite solubility in granitic melts: consequences for the enrichment and fractionation of Nb and Ta in the Earth's crust. *Contrib to Mineral Petrol* 128: 213–227.

Linnen RL, Keppler H. 2002. Melt composition control of Zr/Hf fractionation in magmatic processes. *Geochim Cosmochim Acta* 66: 3293–3301.

Linnen RL, Cuney M. 2005. Granite-related rare-element deposits and experimental constraints on Ta-Nb-W-Sn-Zr-Hf mineralization, in Linnen RL and Samson IM, eds., rare-element geochemistry and mineral deposits. *Geol Assoc Canada, GAC, Short Course*.

López-Moro FJ, López-Plaza M, Gutiérrez-Alonso G, Fernández-Suárez J, López-Carmona A, Hofmann M, *et al*. 2017. Crustal melting and recycling: geochronology and sources of Variscan syn-kinematic anatectic granitoids of the Tormes Dome (Central Iberian Zone). A U–Pb LA-ICP-MS study. *Int J Earth Sci* 107: 1–20.

Losantos E, Borrajo I, Losada I, Boixet L, Castelo Branco JM, Tornos F. 2025. Sn and W mineralisation in the Iberian Peninsula. *Ore Geol Rev* 179: 106542.

Lotout C, Pitra P, Poujol M, Van Den Driessche J. 2017. Ordovician magmatism in the Lévézou massif (French Massif Central): tectonic and geodynamic implications. *Int J Earth Sci* 106: 501–515.

Lotout C, Poujol M, Pitra P, Anczkiewicz R, Van Den Driessche J. 2020. From burial to exhumation: emplacement and metamorphism of mafic eclogitic terranes constrained through multimethod petrochronology, case study from the Lévézou Massif (French Massif Central, Variscan Belt). *J Petrol* 61: egaa046.

Mao J, Ouyang H, Song S. 2019. Geology and Metallogeny of Tungsten and Tin Deposits in China. In *Special Publications of the Society of Economic Geologists*: Mineral Deposits of China.

Marcoux E, Barré B, Pichavant M, Poujol M. 2021. Âge et genèse de la coupole granitique à métaux rares (Sn, Li, Nb-Ta, W) de Montebras (Creuse, Massif central français). *BSGF - Earth Sci Bull* 192: 16.

Marignac C, Cuney M. 1999. Ore deposits of the French Massif Central: insight into the metallogenesis of the Variscan collision belt. *Miner Depos* 34: 472–504.

Martínez Catalán JR, Schulmann K, Ghienne JF. 2021. The Mid-Variscan Allochthon: Keys from correlation, partial retrodeformation and plate-tectonic reconstruction to unlock the geometry of a non-cylindrical belt. *Earth-Sci Rev* 220: 103700.

Melcher F, Graupner T, Gäbler HE, Sitnikova M, Henjes-Kunst F, Oberthür T, *et al*. 2015. Tantalum-(niobium-tin) mineralisation in African pegmatites and rare metal granites: Constraints from Ta-Nb oxide mineralogy, geochemistry and U-Pb geochronology. *Ore Geol Rev* 64: 667–719.

Melleton J, Cocherie A, Faure M, Rossi P. 2010. Precambrian protoliths and Early Paleozoic magmatism in the French Massif

Central: U-Pb data and the North Gondwana connection in the west European Variscan belt. *Gondwana Res* 17: 13–25.

Melleton J, Gloaguen E, Frei D. 2015. Rare-elements (Li-Be-Ta-Sn-Nb) magmatism in the European Variscan Belt, a review. In *SGA 2015 : Ressources minérales dans un monde durable*. Society for Geology Applied to Mineral Deposits, Aug 2015, Nancy, France (https://brgm.hal.science/hal-01156421/).

Merceron T, Vieillard P, Fouillac AM, Meunier A. 1992. Hydrothermal alterations in the Echassieres granitic cupola (Massif Central, France). *Contrib to Mineral Petrol* 112: 279–292.

Mercuzot M. 2020. Reconstitutions paléoenvironnementales et paléoclimatiques en contexte tardi-orogénique: cas des bassins fini-carbonifères à permiens du nord-est du Massif central, France. PhD Thesis, Univ Rennes 1, France, 552 p.

Meyer N, Burisch M, Gutzmer J, Krause J, Scheibert H, Markl G. 2025. Mineral chemistry of the Geyer SW tin skarn deposit : understanding variable fluid / rock ratios and metal fluxes. *Miner Depos* 85–111.

Michaud JAS, Pichavant M, Villaros A. 2021. Rare elements enrichment in crustal peraluminous magmas: insights from partial melting experiments. *Contrib to Mineral Petrol* 176: 96.

Monnier L, Lach P, Salvi S, Melleton J, Bailly L, Beziat D, *et al*. 2018. Quartz trace-element composition by LA-ICP-MS as proxy for granite differentiation, hydrothermal episodes, and related mineralization: The Beauvoir Granite (Echassières district), France. *Lithos* 320: 355–377.

Monnier L, Salvi S, Melleton J, Bailly L, Béziat D, de Parseval P, *et al*. 2019. Multiple generations of wolframite mineralization in the Echassieres district (Massif Central, France). *Minerals* 9: 637.

Monnier L, Salvi S, Jourdan V, Sall S, Bailly L, Melleton J, *et al*. 2020. Contrasting fluid behavior during two styles of greisen alteration leading to distinct wolframite mineralizations: The Echassières district (Massif Central). *Ore Geol Rev* 124: 103648.

Monnier L, Melleton J, Vanderhaeghe O, *et al*. 2021. Episodic precipitation of wolframite during an orogen: the echassières district, Variscan belt of France. *Minerals* 11: 923.

Monnier L, Salvi S, Melleton J, Lach P, Pochon A, Bailly L, *et al*. 2022. Mica trace-element signatures: Highlighting superimposed W-Sn mineralizations and fluid sources. *Chem Geol* 600: 120866.

Moyen JF, Laurent O, Chelle-Michou C, Couzinié S, Vanderhaeghe O, Zeh A, *et al*. 2017. Collision *vs*. subduction-related magmatism: Two contrasting ways of granite formation and implications for crustal growth. *Lithos* 277: 154–177.

Moyen JF. 2009. High Sr/Y and La/Yb ratios: The meaning of the "adakitic signature." *Lithos* 112: 556–574.

Palme H, O'Neill H. 2014. Cosmochemical Estimates of Mantle Composition. *Treatise Geochemistry*, 2nd Ed.

Passos Do Carmo C, Vanderhaeghe O, Laurent O, Berger J, Bellanger M, Leisen M, *et al*. 2025. Petrogenetic link between late Ediacarian metasedimentary rocks and Variscan migmatites and granitoids in the Pontgibaud area, French Massif Central-implications for the crustal structure. *BSGF - Earth Sci Bull* 196 : 13.

Paton C, Woodhead JD, Hellstrom JC, Hergt JM, Greig A, Maas R. 2010. Improved laser ablation U-Pb zircon geochronology through robust downhole fractionation correction. *Geochemistry, Geophys Geosystems* 11: Q0AA06.

Petrus JA, Kamber BS. 2012. VizualAge: A novel approach to laser ablation ICP-MS U-Pb geochronology data reduction. *Geostand Geoanalytical Res* 36: 247–270.

Pin C. 1991. Sr-Nd isotopic study of igneous and metasedimentary enclaves in some Hercynian granitoids from the Massif Central, France. In *Enclaves and granite petrology*: 333–343.

Pin C, Paquette JL. 1997. A mantle-derived bimodal suite in the Hercynian Belt: Nd isotope and trace element evidence for a subduction-related rift origin of the Late Devonian Brevenne metavolcanics, Massif Central (France). *Contrib to Mineral Petrol* 129: 222–238.

Poujol M, Hallot E, Abiven B, Poulizac A. 2024. Zircon and apatite U-Pb geochronology of the Paleoproterozoic (Eburnean) basement and late Neoproterozoic (Pan-African) metamorphism and magmatism from Port-Béni, Armorican Massif (France). *BSGF - Earth Sci Bull* 195: 10.

Putzolu F, Seltmann R, Dolgopolova A, Armstrong RN, Shail RK, Spratt J, *et al*. 2024. Influence of magmatic and magmatic-hydrothermal processes on the lithium endowment of micas in the Cornubian Batholith (SW England). *Miner Depos* 59: 1067–1088.

Quenardel JM, Santallier D, Burg JP, Bril H, Cathelineau M, Marignac C. 1991. Le Massif central/the Central Massif. *Sci Géologiques, Bull mémoires* 44: 105–206.

Raimbault L, Azencott C. 1987. Géochimie des éléments majeurs et traces du granite à métaux rares de Beauvoir. *Géologie Fr*: 2–3.

Raimbault L, Cuney M, Azencott C, Duthou JL, Joron JL. 1995. Geochemical evidence for a multistage magmatic genesis of Ta-Sn-Li mineralization in the granite at Beauvoir, French Massif Central. *Econ Geol* 90: 548–576.

Ravier J, Chenevoy M. 1979. Présence de formations granulitiques jalonnant un linéament crustal dans la série cristallophyllienne de la Sioule (Massif central français). *Comptes Rendus l'Académie des Sci Paris - Série D*: 1704–1706.

Reinhardt N, Gerdes A, Beranoaguirre A, Frenzel M, Meinert LD, Gutzmer J, *et al*. 2022. Timing of magmatic-hydrothermal activity in the Variscan Orogenic Belt: LA-ICP-MS U–Pb geochronology of skarn-related garnet from the Schwarzenberg District, Erzgebirge. *Miner Depos* 57: 1071–1087.

Rocher O, Ballouard C, Richard A, *et al*. 2024. Unravelling the magmatic and hydrothermal evolution of rare-metal granites through apatite geochemistry and geochronology: The Variscan Beauvoir granite (French Massif Central). *Chem Geol* 670: 122400.

Romer RL, Kroner U. 2015. Sediment and weathering control on the distribution of Paleozoic magmatic tin–tungsten mineralization. *Miner Depos* 50: 327–338.

Romer RL, Kroner U. 2016. Phanerozoic tin and tungsten mineralization—Tectonic controls on the distribution of enriched protoliths and heat sources for crustal melting. *Gondwana Res* 31: 60–95.

Samson IM, Sinclair WD. 1992. Magmatic hydrothermal fluids and the origin of quartz-tourmaline orbicules in the Seagull Batholith, Yukon Territory. *Can Mineral* 30: 937–954.

Sawyer EW. 2008. Working with migmatites: nomenclature for the constituent parts. *Mineral Assoc Canada, short course Ser* 38: 1–28.

Schmidt C, Romer RL, Wohlgemuth-Ueberwasser CC, Appelt O. 2020. Partitioning of Sn and W between granitic melt and aqueous fluid. *Ore Geol Rev* 117: 103263.

Schulmann K, Edel JB, Martínez Catalán JR, Mazur S, Guy A, Lardeaux JM, *et al*. 2022. Tectonic evolution and global crustal architecture of the European Variscan belt constrained by geophysical data. *Earth-Sci Rev* 234: 104195.

Schulz B. 2009. EMP-monazite age controls on PT paths of garnet metapelites in the Variscan inverted metamorphic sequence of La Sioule, French Massif Central. *Bull la Société géologique Fr* 180: 271–282.

Schulz B, Triboulet C, Audren C, Feybesse JL. 2001. PT-paths from metapelite garnet zonations, and crustal stacking in the Variscan inverted metamorphic sequence of La Sioule, French Massif Central. *Zeitschrift-Deutschen Geol Gesellschaft* 152: 1–26.

Silva D, Groat L, Martins T, Linnen R. 2023. Structural controls on the origin and emplacement of lithium-bearing pegmatites. *Can J Mineral Petrol* 61: 1053–1062.

Simons B, Shail RK, Andersen JC. Ø. 2016. The petrogenesis of the Early Permian Variscan granites of the Cornubian Batholith: Lower plate post-collisional peraluminous magmatism in the Rhenohercynian Zone of SW England. *Lithos* 260: 76–94.

Sinclair WD, Gonevchuk GA, Korostelev PG, Semenyak BI, Rodionov SM, Seltmann R, *et al*. 2014. World Tin and Tungsten Deposit database. *Geol Surv Canada Open File*: 7688.

Smithies RH, Lu Y, Champion DC, *et al*. 2025. Giant lithium-rich pegmatites in Archean cratons form by remelting refertilised roots of greenstone belts. *Commun Earth Environ* 6: 630.

Stacey JS, Kramers JD. 1975. Approximation of terrestrial lead isotope evolution by a two-stage model. *Earth Planet Sci Lett* 26: 207–221.

Stepanov AS, Hermann J. 2013. Fractionation of Nb and Ta by biotite and phengite: Implications for the "missing Nb paradox." *Geology* 41: 303–306.

Stephan T, Kroner U, Romer RL. 2019. The pre-orogenic detrital zircon record of the Peri-Gondwanan crust. *Geol Mag* 156: 281–307.

Sweetapple MT, Collins PLF. 2002. Genetic framework for the classification and distribution of Archean rare metal pegmatites in the North Pilbara Craton, Western Australia. *Econ Geol* 97: 873–895.

Thiéry V. 2012. La série de la Sioule, 75 ans après les travaux de J. Richard (1938). Historique des études géologiques et évolution des concepts. *Rev Des Sci Nat D'auvergne* 76: 73–91.

Thiery V, Rolin P, Marquer D, Cocherie A, Mark Fanning C, Rossi P. 2009. Visean sinistral wrench faulting along the sillon houiller in the french massif central: Late variscan tectonic implications. *Bull la Soc Geol Fr* 180: 513–528.

Tichomirowa M, Sergeev S, Hans-Jürgen B, Dietmar L. 2012. Inferring protoliths of high-grade metamorphic gneisses of the Erzgebirge using zirconology, geochemistry and comparison with lower-grade rocks from Lusatia (Saxothuringia, Germany). *Contrib to Mineral Petrol* 164: 375–396.

Tichomirowa M, Käßner A, Sperner B, Lapp M, Leonhardt D, Linnemann U. 2019. Dating multiply overprinted granites: The effect of protracted magmatism and fluid flow on dating systems (zircon U-Pb: SHRIMP/SIMS, LA-ICP-MS, CA-ID-TIMS; and Rb–Sr, Ar–Ar)–Granites from the Western Erzgebirge (Bohemian Massif, Germany). *Chem Geol* 519: 11–38.

Turpin L, Cuney M, Friedrich M, Bouchez JL, Aubertin M. 1990. Meta-igneous origin of Hercynian peraluminous granites in N.W. French Massif Central: implications for crustal history reconstructions. *Contrib to Mineral Petrol* 104: 163–172.

Vallance J, Cathelineau M, Marignac C, Boiron MC, Fourcade S, Martineau F, *et al*. 2001. Microfracturing and fluid mixing in granties: W-(Sn) ore deposition at Vaulry (NW French Massif Central). *Tectonophysics* 336: 43–61.

Vanderhaeghe O, Laurent O, Gardien V, Moyen JF, Gébelin A, Chelle-Michou C, *et al*. 2020. Flow of partially molten crust controlling construction, growth and collapse of the Variscan orogenic belt: The geologic record of the French Massif Central. *BSGF - Earth Sci Bull* 191: 25.

Vennat G. 1982. Un exemple de relations volcanisme–plutonisme : chronologie, pétrologie, dynamisme d'un complexe volcano-plutonique dans la région de Gannat–Les Ancizes (Massif central français). PhD Thesis, Univ Clermont-Ferrand, France, 155 p.

Vermeesch P. 2018. IsoplotR: A free and open toolbox for geochronology. *Geosci Front* 9: 1479–1493.

Vigneresse JL. 1987. Organisation tridimensionnelle du massif d'Echassières et bilan des mesures géophysiques de surface. *Géologie la Fr*: 27–32.

Villa IM, De Bièvre P, Holden NE, Renne PR. 2015. IUPAC-IUGS recommendation on the half life of ^{87}Rb. *Geochim Cosmochim Acta* 164: 382–385.

Villaseca C, Barbero L, Herreros V. 1998. A re-examination of the typology of peraluminous granite types in intracontinental orogenic belts. *Earth Environ Sci Trans R Soc Edinburgh* 89: 113–119.

Warr LN. 2021. IMA–CNMNC approved mineral symbols. *Mineral Mag* 85: 291–320.

Werle M, Stevens G, Moyen JF, Laurent O, Harris C, Lana CC, *et al*. 2023. Cryptic crustal growth identified through Variscan post-collisional lamprophyre-granite composite dykes, French Massif Central. *Lithos* 454–455: 107270.

Wolf M, Romer RL, Franz L, López-moro FJ. 2018. Tin in granitic melts : The role of melting temperature and protolith composition. *Lithos* 310–311: 20–30.

Zhang R, Lehmann B, Seltmann R, Sun W, Li C. 2017. Cassiterite U-Pb geochronology constrains magmatic-hydrothermal evolution in complex evolved granite systems: The classic Erzgebirge tin province (Saxony and Bohemia). *Geology* 45: 1095–1098.

Zhao P, Chu X, Williams-Jones AE, Mao J, Yuan S. 2022a. The role of phyllosilicate partial melting in segregating tungsten and tin deposits in W-Sn metallogenic provinces. *Geology* 50: 121–125.

Zhao P, Yuan S, Williams-Jones AE, Romer RL, Yan C, Song S, *et al*. 2022b. Temporal separation of W and Sn mineralization by temperature-controlled incongruent melting of a single protolith: evidence from the Wangxianling area, Nanling Region, South China. *Econ Geol* 117: 667–682.

Cite this article as: Ballouard C, Carr PA. Monnier L, Fidalgo J-C, Rocher O, Esteves N, Laurent O, Daoulas-Gérardin M, Peiffert C, Declercq L, Mercadier J, Plunder A, Melleton J. 2026. Rare-metal mineralization and crust-derived magmatism in a collisional orogen: the Variscan metallogenic odyssey of the Sioule region (French Massif Central), *BSGF - Earth Sciences Bulletin* 197: 12. https://doi.org/10.1051/bsgf/2026003